Cellular and Molecular Life Sciences (2023) 80:256
https://doi.org/10.1007/s00018-023-04906-5

ORIGINAL ARTICLE

AUF1-induced circular RNA hsa_circ_0010467 promotes platinum resistance of ovarian cancer through miR-637/LIF/STAT3 axis

Yangjun Wu[1,2] · Miao Xu[3] · Zheng Feng[1,2] · Hao Wu[4] · Jingni Wu[4] · Xinyu Ha[1,2] · Yong Wu[1,2] · Siyu Chen[1,2] · Fei Xu[1,2] · Hao Wen[1,2] · Shengli Li[4] · Xiaohua Wu[1,2]

Received: 12 March 2023 / Revised: 12 July 2023 / Accepted: 2 August 2023 / Published online: 17 August 2023

Abstract

Background Increasing evidences has indicated that primary and acquired resistance of ovarian cancer (OC) to platinum is mediated by multiple molecular and cellular factors. Understanding these mechanisms could promote the therapeutic efficiency for patients with OC.

Methods Here, we screened the expression pattern of circRNAs in samples derived from platinum-resistant and platinum-sensitive OC patients using RNA-sequencing (RNA-seq). The expression of hsa_circ_0010467 was validated by Sanger sequencing, RT-qPCR, and fluorescence in situ hybridization (FISH) assays. Overexpression and knockdown experiments were performed to explore the function of hsa_circ_0010467. The effects of hsa_circ_0010467 on enhancing platinum treatment were validated in OC cells, mouse model and patient-derived organoid (PDO). RNA pull-down, RNA immunoprecipitation (RIP), and dual-luciferase reporter assays were performed to investigate the interaction between hsa_circ_0010467 and proteins.

Results Increased expression of hsa_circ_0010467 is observed in platinum-resistant OC cells, tissues and serum exosomes, which is positively correlated with advanced tumor stage and poor prognosis of OC patients. Hsa_circ_0010467 is found to maintain the platinum resistance via inducing tumor cell stemness, and silencing hsa_circ_0010467 substantially increases the efficacy of platinum treatment on inhibiting OC cell proliferation. Further investigation reveals that hsa_circ_0010467 acts as a miR-637 sponge to mediate the repressive effect of miR-637 on leukemia inhibitory factor (LIF) and activates the LIF/STAT3 signaling pathway. We further discover that AUF1 could promote the biogenesis of hsa_circ_0010467 in OC.

Conclusion Our study uncovers the mechanism that hsa_circ_0010467 mediates the platinum resistance of OC through AUF1/hsa_circ_0010467/miR-637/LIF/STAT3 axis, and provides potential targets for the treatment of platinum-resistant OC patients.

Keywords Platinum resistance · Ovarian cancer · Hsa_circ_0010467 · EIF4G3 · AUF1 · miR-637 · LIF

Introduction

Ovarian cancer (OC) is considered to be one of the most lethal gynaecologic malignancies worldwide [1]. The majority (> 80%) of OC are diagnosed at advanced stages

Yangjun Wu, Miao Xu and Zheng Feng authors contributed equally to this work.

✉ Shengli Li
shengli.li@sjtu.edu.cn

✉ Xiaohua Wu
wu.xh@fudan.edu.cn

1 Department of Gynecologic Oncology, Fudan University Shanghai Cancer Center, Fudan University, Shanghai, China

2 Department of Oncology, Shanghai Medical College, Fudan University, Shanghai, China

3 Department of Clinical Nutrition, West China Hospital, Sichuan University, Chengdu, China

4 Precision Research Center for Refractory Diseases, Institute for Clinical Research, Shanghai General Hospital, Shanghai Jiao Tong University School of Medicine, Shanghai 201620, China

when tumor has spread to the peritoneal cavity and upper abdominal organs [2], which substantially reduces the chance to cure this malignancy. The most active therapeutic agents against OC are cytoreductive surgery followed by platinum-based chemotherapy. Recurrence of cancer after initial platinum-based chemotherapy is very common in OC patients, which is mainly due to the development of platinum resistance [3]. Thus, understanding the molecular basis of OC platinum resistance and developing new effective therapies are urgent.

Circular RNAs (circRNAs), which are a newly discovered class of noncoding RNAs, are generated from unique back-splicing of pre-mRNAs that form covalently closed transcripts [4]. With the development and utilization of deep RNA sequencing and related computational algorithms, circRNAs have been demonstrated to be widespread in human transcriptome. Accumulating studies have shown that circRNAs are aberrantly expressed in tumors and play critical roles in cancer growth, metastasis, stemness and resistance to anti-tumor therapy [5–8]. Given their unique biological structure and functions, identification of circRNAs with high specificity and sensitivity will provide opportunities for the early diagnosis, clinical treatment, and prognosis monitoring of patients with OC [9]. To date, several OC-related circRNAs have been reported. For example, the ectopic expression of circMUC16 in OC tissues strikingly facilitated invasion and metastasis of OC cells in vitro and in vivo via binding to miR-199a-5p and upregulating the expression of Beclin1 and RUNX1. In turn, RUNX1 elevated the expression of circMUC16 by promoting its transcription [10]. More recently, Zhang et al. revealed that circPLEKHM3 functioned as a tumor suppressor in OC cells and inhibited cell growth, migration and epithelial-mesenchymal transition (EMT) by targeting the miR-9/BRCA1/DNAJB6/KLF4/AKT1 axis [11]. CircCdr1as was demonstrated to increase the sensitivity of OC cells to cisplatin by regulating the miR-1270/SCAI signaling pathway [12]. However, further exploration is needed to elucidate the underlying mechanisms how circRNAs mediate the platinum resistance of OC patients.

In the present study, we comparatively analyzed the expression profile of circRNAs in platinum-resistant and platinum-sensitive OC tissues, and found that hsa_circ_0010467 was up-regulated in platinum-resistant OC and positively related to advanced tumor stage and poor prognosis. We found that hsa_circ_0010467 mediated cancer stemness and maintained platinum resistance by sponging miR-637, thereby activating the LIF/STAT3 signaling pathway. Moreover, AUF1 could regulate the biogenesis of hsa_circ_0010467. Our findings provided insights into the mechanism of maintaining platinum resistance of OC cancer cells.

Materials and methods

Collections of ovarian tissues

The OC tissues and serum samples were obtained from the Department of Gynecologic Oncology, Fudan University Shanghai Cancer Center (FUSCC). This study was approved by the Clinical Research Ethics Committee of Fudan University Shanghai Cancer Center. Written informed consents were obtained from all patients. This study was conducted in accordance with the ethical guidelines of the Declaration of Helsinki. Three pathologists confirmed the pathological diagnosis of epithelial OC. Patients who initially respond to platinum-based chemotherapy and subsequently relapse ≥ 6 months after initial treatment are classified as "platinum sensitive". Patients who relapse within 6 months of completing platinum-based therapy are classified as "platinum resistant" and typically have low response rates to subsequent chemotherapy. In addition, patients with R0 excision ($n = 67$) were collected in this study. The median platinum free interval (PFI) of patients with platinum sensitive recurrent ovarian cancer is 16.2 months, and the PFI of patients with platinum resistant recurrent ovarian cancer is 3.5 months. The clinical and pathological characteristics of OC patients were provided in Supplementary Table S1.

RNA sequencing and circRNA identification

RNA sequencing (RNA-seq) was performed according to the manufacturer's instructions [13]. Briefly, total RNA was extracted by the Trizol reagent (Invitrogen, Carlsbad, CA, USA) from platinum-resistant and platinum-sensitive OC tissues. Detailed clinical and pathological characteristics of patients whose samples were used for RNA sequencing were provided in Supplementary Table S2. The RbioMinus Eukaryote kit (Qiagen, Valencia, CA, USA) was used to remove ribosome RNAs (rRNA) from the total RNA samples. The rRNA-depleted RNA samples were fragmented and subject to cDNA synthesis with random hexamer primers. Then, the End-It DNA End Repair kit was used to repair the ends, an A was added to the repaired 3′ ends, and adapter sequences were ligated with cDNA fragments. Finally, purified RNA libraries were subject to a HiSeq 3000 sequencer (Illumina, San Diego, CA, USA). All raw RNA-seq data were deposited in the Gene Expression Omnibus (GEO) database with the accession number of GSE214302.

Raw RNA-seq reads were first trimmed by the Trimmomatic software (version 0.39) [14] to remove adapters and low-quality reads. Trimmed reads were then mapped to

the human reference genome (GRCh38) by using HISAT2 (version 2.2.1) [15]. Unmapped reads were then extracted from alignments by SAMtools [16]. These unmapped reads were utilized to call back-splicing junctions that form circRNAs. To obtain reliable circRNA candidates, four different algorithms were employed to identify circRNAs, including find_circ [17], circRNA_finder [18], CIRI2 [19], and CIRCexplorer2 [20]. In each sample, circRNAs that were detected by at least two methods with ≥ 2 back-splicing reads were kept for following analysis. For each circRNA, an average number of back-splicing reads in all detectable tools were calculated as the raw expression level in certain samples. Raw expression levels were normalized by the total reads in each sample. These circRNAs were annotated with their host genes through coordinate intersection by using the BEDTools software [21]. In addition, raw counts of circRNAs were utilized to performed differential expression analysis by using DESeq2 [22]. CircRNAs with fold change > 1.5 and FDR < 0.05 were considered as significantly differentially expressed. Gene-level expression were calculated by the StringTie program (version 2.1.4) [23] and normalized to the unit of Transcripts per kilobase Per Million mapped reads (TPM).

Gene set enrichment analysis

The genes in hsa_circ_0010467 knockdown and control samples were ranked by normalized expression levels. Ranked genes were subject to the gene set enrichment analysis (GSEA) to identify enriched hallmark biological processes. The GSAE analysis was performed by the clusterProfiler R package [24]. The gene sets of 50 hallmarks were retrieved from the Molecular Signature Database (MSigDB) database [25].

Cell culture

SKOV3 and A2780 cell lines were purchased from the American Type Culture Collection (ATCC, Manassas, VA, USA). The HEK293T cell line was obtained from the Chinese Academy of Sciences (Shanghai, China). Cell lines were authenticated by short tandem repeat (SRT) profiling. Mycoplasma contamination was regularly examined using the Lookout Mycoplasma PCR Detection Kit (Sigma Aldrich, USA). To establish ovarian cancer cells resistant to cisplatin (DDP) (Selleck, Houston, TX, USA), SKOV3 and A2780 underwent continuous stepwise exposure to increasing concentrations of cisplatin to create the cisplatin-resistant cell lines, SKOV3-DDP and A2780-DDP.

Plasmid construction, RNAi and cell transfection

The siRNAs that target hsa_circ_0010467 splicing sites were designed and synthesized by RiboBio (RiboBio Biotechnology, Guangzhou, China). Transfection of plasmids, siRNA, or miRNA mimics or inhibitors (RiboBio Biotechnology, Guangzhou, China) was performed using Oligofectamine transfection reagent (Invitrogen, Carlsbad, CA) according to the manufacturer's instructions. The sequences of siRNAs against specific targets are listed in Supplemental Table S3. The shRNAs targeting hsa_circ_0010467, AUF1 and EIF4A3 were synthesized by TSINGKE (Shanghai, China), and were cloned into a vector (lenti-gRNA-puro). To construct hsa_circ_0010467 overexpression vector, the full length of human hsa_circ_0010467 was inserted into the pLCDH-ciR vector (Geenseed Biotech, Guangzhou, China), which contained a front and back circular frame, whereas the mock vector with no hsa_circ_0010467 sequence was used as a control. To construct LIF overexpression vector, the open reading frame (ORF) of human LIF was inserted into the PCDH-3 × Flag vector. Stable cell lines were screened by administration of puromycin (Yeasen Biotech, Shanghai, China). The plasmids were transfected into ovarian cancer cells using HieffTrans™ Liposomal Transfection Reagent (Yeasen Biotech, Shanghai, China) according to the manufacturer's instructions. The primers used for cloning are listed in Supplementary Table S4.

Nuclear and cytoplasmic extraction

Nuclear and cytoplasmic fractions were separated by a PARIS™ cytoplasmic and nuclear extraction kit (Life Technologies, MA, USA) following the manufacturer's instructions. β-actin and U2 were used as cytoplasmic and nuclear positive controls, respectively.

Cell proliferation, colony formation, EdU and spheroid formation assays

Cell proliferation was evaluated by Cell Counting Kit 8 (CCK-8), EdU, and colony formation assays. Briefly, ovarian cancer cells were plated at 1×10^3 cells per well in 96-well plates and incubated overnight in DMEM medium supplemented with 10% FBS. Then, 10 µl CCK-8 was added to the test well and incubated for 2 h. Absorbance was then measured at a wavelength of 450 nm. For EdU assay, cells were treated with or without cisplatin for 24 h and then incubated with EdU (10 µM) before fixation. Cellular DNA staining using Hoechst 33342 (Beyotime, Shanghai, China). Cell proliferation was detected under a fluorescence microscope. In colony formation assay, OC cells were seeded at 1×10^3 cells/well in 6-well plates and cultured in DMEM medium supplemented with 10% FBS for two weeks. Colony

formation was determined by counting the number of stained colonies by crystal violet. CSCs self-renewal ability was evaluated by spheroid formation assay. In brief, 1×10^3 cells/well were seeded in ultra-low attachment 6-well culture plates (Corning, NY, USA). Spontaneously generated spheroids were cultured in serum-free DMEM/F12 medium supplemented with 2% B-27 supplement (Invitrogen, Carlsbad, CA, USA), 20 ng/mL basic fibroblast growth factor (FGF, Peprotech, Rocky Hill, NJ, USA), and 20 ng/mL epidermal growth factor (EGF, Peprotech, Rocky Hill, NJ, USA). After two weeks, the spheroids were photographed with a fluorescence microscope and collected by gentle centrifugation for western blotting or RT-qPCR analysis. For the drug sensitivity assay, OC cells were seeded in 96-well plates (5×10^3 cells/well) for 24 h, and the cells were treated with cisplatin at the indicated doses for 48 h. After incubation with 10 µl CCK-8 at 37 °C for 2 h, the absorbance was then measured at a wavelength of 450 nm.

Establishment of patient-derived organoids

Patient-derived organoids (PDOs) were established from specimens that were collected by platinum-resistant OC ascites. Organoids were established as previously described with appropriate adjustments [26]. Ascites effusion samples were centrifuged at 1,500 r.p.m. for 3 min, and the supernatant was removed. Then these samples were treated with 2 ml red blood cell lysis buffer for 5 min at room temperature. If ascites contained a small amount of solid tissue, filtrate was first filtered with 100 µm filter membrane to collect filtrate, and then centrifuged. Afterwards, erythrocyte lysis and 10 ml $AdDF^{+++}$ (Advanced DMEM/F12 containing 1 × Glutamax, 10 mM HEPES and antibiotics) were added and suspension was centrifuged at 1,000 r.p.m. The prepared cells were coated in Matrigel (Corning, NY, USA), supplied with ovarian cancer organoid growth medium (Yeasen Biotechnology, Shanghai, China) every 3 to 4 days, and incubated at 5% CO_2. Phase-contrast images were taken using CKX41 (Olympus, Japan). Detailed clinical characteristics of OC patients where PDOs were derived were provided in Supplementary Table S5.

Dual luciferase reporter assay

Wild-type and mutant hsa_circ_0010467 and LIF fragments (hsa_circ_0010467-Mut or LIF-Mut) were synthesized and cloned into dual luciferase reporter plasmids (Promega, USA) containing the psiCheck2 promoter. After OC cells were inoculated into a 24-well plate and cultured for 24 h, they were co-transfected with the wild-type or mutant reporter gene plasmids and overexpression or silencing plasmid mimics. After 48 h, luciferase activities were measured using the Dual-Luciferase Reporter Assay System (Promega, USA). The primers used for cloning were provided in Supplementary Table S4.

RNA pull-down assay

A2780-DDP and SKOV3-DDP cells were harvested and lysed, and M280 streptavidin Dynabeads (Invitrogen, USA) were incubated with the biotinylated-hsa_circ_0010467 probe (RiboBio Biotechnology, Guangzhou, China) at room temperature for 2 h to generate probe-coated beads. The cell lysates were then incubated with the probe/bead complexes at 4 °C overnight. Subsequently, the RNA complexes bound to the beads were eluted and extracted with Trizol reagent (Invitrogen, Carlsbad, CA, USA) for RT-qPCR analysis. The biotinylated-hsa_circ_0010467 probe used for RNA pull-down assay were provided in Supplementary Table S3.

RNA immunoprecipitation

The RNA immunoprecipitation (RIP) assay was conducted using a Magna RIP Kit (Millipore, Billerica, MA, USA) in accordance with the manufacturer's instructions. The antibodies for the RIP assays included Flag, AUF1, and IgG (Cell Signaling Technology, Danvers, MA, USA). Information of these antibodies is listed in Supplementary Table S6.

Western blot analysis

Proteins were subject to SDS-PAGE and transferred to the nitrocellulose membranes (GE, CT, USA). After being blocked by non-fat milk, the membrane was incubated with primary antibodies followed by the incubation of the secondary antibodies. The band density was analyzed using ImageJ and compared with the internal control. Information of used antibodies is listed in Supplementary Table S6.

Animal experiments

Four-week-old female BALB/c nude mice were purchased from the SLAC (Shanghai, China) and housed under pathogen-free conditions. A2780-DDP cells (5×10^6) were subcutaneously injected into the dorsal flank of each mouse, and the tumor volume and weight of mice were monitored and recorded. Four weeks after injection, the mice were sacrificed. Tumor volume was calculated according to the formula: volume = (width^2 × length)/2. For in vivo drug experiments, two weeks after cells injection, DDP or 5% glucose solution was administered by intraperitoneal (ip) injection at the dose of 5 mg/kg. All animal experiments were allowed in the light of NIH Guidelines for the Care and Use of Laboratory Animals and approved by the Animal Care Committee of Fudan University.

Statistical analysis

Each experiment was repeated at least three times. Statistical analysis was performed using GraphPad Prism 8.0 software, and $P < 0.05$ was considered statistically significant ($^{*}P < 0.05$, $^{**}P < 0.01$, $^{***}P < 0.001$, and $^{****}P < 0.0001$). The experimental data was expressed as the means ± SEM values. Two-sided Student's t-test was used to evaluate differences between two groups, and one-way analysis of variance (ANOVA) was used to evaluate differences among multiple groups.

Results

Hsa_circ_0010467 is upregulated in platinum-resistant OC tissues

To identify circRNAs that play crucial roles in maintaining the platinum resistance of OC, we performed RNA-seq in tissues derived from platinum-resistant (n = 8) and platinum-sensitive (n = 10) OC patients (see Methods). We performed hierarchical clustering of all samples with the expression profile of variable mRNAs, the platinum-sensitive and platinum-resistant samples were clustered together, respectively (Supplementary Figure S1A). We further performed DEG analysis between samples derived from platinum-resistant and platinum-sensitive OC patients (Supplementary Table S7). These DEGs were enriched in RNA processing and epigenetic regulation-related biological processes (Supplementary Figure S1B). In total, 53 circRNAs showed downregulation and 16 circRNAs were upregulated in platinum-resistant OC samples (Fig. 1A and Supplementary Table S8). We then established cisplatin-resistant A2780 and SKOV3 cell lines (A2780-DDP, SKOV3-DDP) (Supplementary Figure S2A) to further validate reliable candidate circRNAs. The expression of top 5 up-regulated circRNAs in resistant tissues (named hsa_circ_0010467, hsa_circ_0002782, hsa_circ_0004220, hsa_circ_0069227, and hsa_circ_0000067 in the circBase database [27]) were compared between platinum-resistant OC cells and the parental cells (Supplementary Figure S2B). The expression changes of these circRNAs were consistent with those in the RNA-seq data (Supplementary Figure S2C). Among these circRNAs, hsa_circ_0010467 showed the largest fold change in resistant tissues or cells (Supplementary Figure S2C), and hsa_circ_0010467 knockdown exhibited the largest effect of cell proliferation inhibition under cisplatin treatment (Supplementary Figure S2D and S2E). Hsa_circ_0010467 was generated from the tail-to-end splicing of exon 9, 10, 11, 12, and 13 of the EIF4G3 gene (Fig. 1B). Hsa_circ_0010467 is 1,430 nt long and owns it unique junction (between exon 9 and 13), which was further validated by Sanger sequencing in A2780-DDP cells (Fig. 1B). Hsa_circ_0010467 was the predominant circRNA compared to hsa_circ_0010466 (a circRNA derived from exon 12 and 13 of EIF4G3) and hsa_circ_0007214 (a circRNA derived from exon 10, 11, 12, and 13 of EIF4G3) in OC cells (Supplementary Figure S2F). Hsa_circ_0010467 was further validated by RT-qPCR using convergent and divergent primers, wherein divergent primers generated a specific divergent band from cDNA but not gDNA (Fig. 1C). Furthermore, hsa_circ_0010467 showed significantly higher stability than linear EIF4G3 mRNA after treatment of RNaseR (Fig. 1D) and actinomycin D (Supplementary Figure S3A) in A2780-DDP and SKOV3-DDP cells. To determine the intracellular distribution of hsa_circ_0010467, we performed fluorescence in situ hybridization (FISH) and the nucleocytoplasmic fractionation experiment, and found that hsa_circ_0010467 distributed in both the nucleus and cytoplasm of the A2780-DDP and SKOV3-DDP cells (Fig. 1E and F). Hsa_circ_0010467 showed the highest expression levels in cisplatin-resistant cells (A2780-DDP and SKOV3-DDP cells) across 12 OC cell lines (Fig. 1G), whereas linear EIF4G3 mRNA was remarkably down-regulated in cisplatin-induced resistant cell lines (Fig. 1H). These results indicated that hsa_circ_0010467 might play important roles in the induction and maintenance of cisplatin resistance in OC cells.

To investigate the clinical relevance of hsa_circ_0010467 in OC, we further examined the expression of hsa_circ_0010467 and its association with the clinicopathological characteristics of OC patients (Supplementary Table S1). Hsa_circ_0010467 was significantly upregulated in platinum-resistant patients in two different OC cohorts (Fig. 1I and Supplementary Figure S3B). OC patients with high level of hsa_circ_0010467 exhibited shorter overall survival time (Fig. 1J) and advanced tumor stage (Fig. 1K). We further examined that expression of hsa_circ_0010467 and EIF4G3 mRNA in primary tumors from 7 OC patients with platinum-resistant relapse and 7 OC patients with platinum-sensitive relapse. Our analysis found that hsa_circ_0010467 was significantly upregulated in platinum-resistant relapsed OC ($P = 0.027$), but showed no remarkable change in platinum-sensitive relapsed OC ($P = 0.077$) tissues (Fig. 1L). The linear EIF4G3 mRNA showed no significant changes in neither platinum-resistant nor platinum-sensitive relapsed OC tissues (Supplementary Figure S3C). Exosomes in human circulating systems, which contains a variety of molecules (including DNA, RNA, proteins, lipids, and metabolites), have been widely used in liquid biopsy for early screening, diagnosis, and treatment of tumors [28–30]. We next examined the expression level of hsa_circ_0010467 in plasma exosomes of platinum-resistant and platinum-sensitive OC patients. Plasma exosomes of those patients were exacted and assessed by western blotting and transmission electron

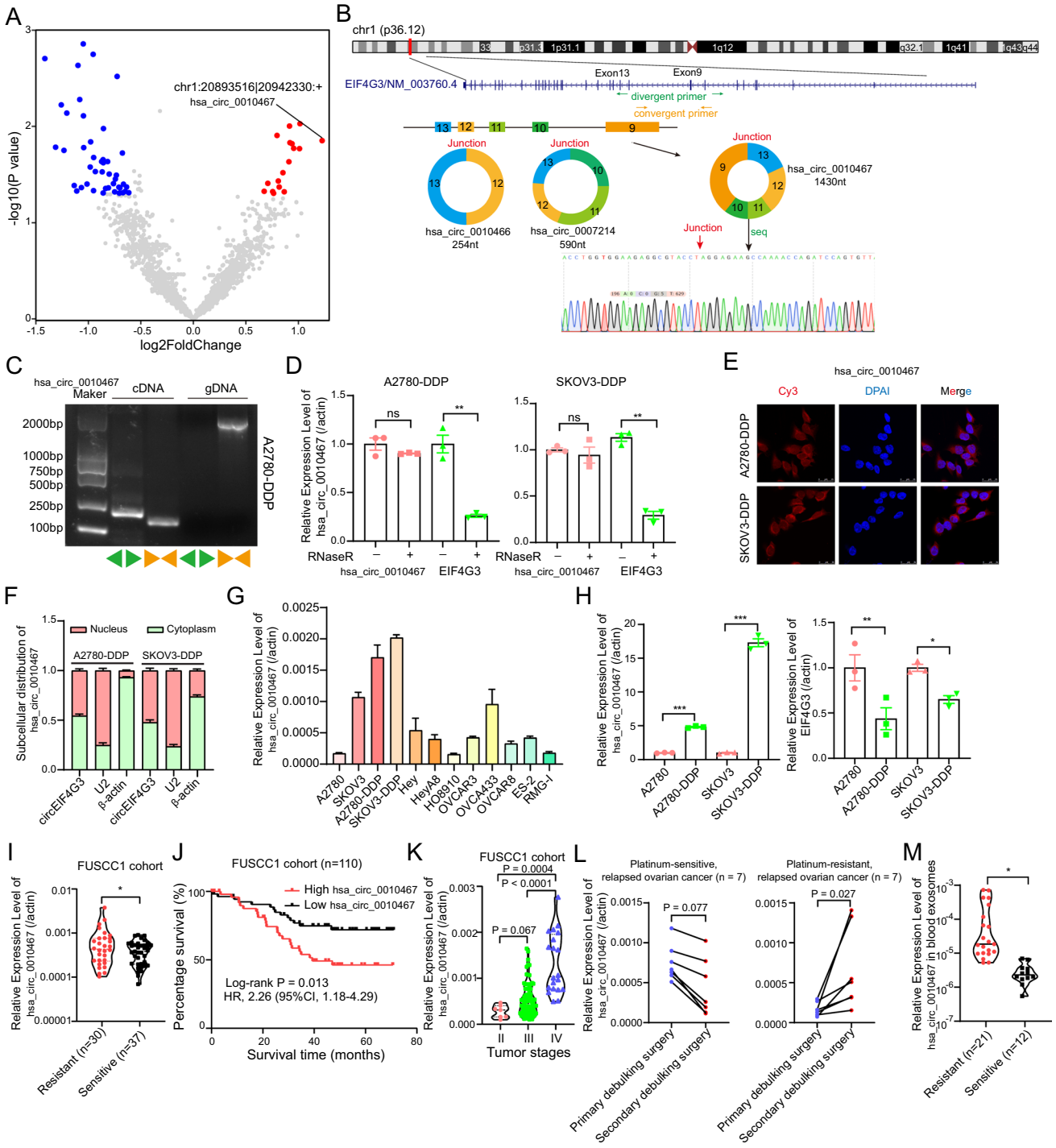

microscopy (TEM) (Supplementary Figure S3D and S3E). Plasma exosomal hsa_circ_0010467 levels in the platinum-resistant remarkably increased, compared to those in the platinum-sensitive OC patients (Fig. 1M). Taken together, these results demonstrated that hsa_circ_0010467 was frequently up-regulated in platinum-resistant OC and could be a candidate plasma marker for predicting the prognosis and platinum resistance development of OC patients.

Hsa_circ_0010467 promotes the proliferation of OC cells and self-renewal maintenance of ovarian CSC

To further explore the influence of hsa_circ_0010467 on OC cells, two shRNAs targeting the junction sites were designed (Fig. 2A and Supplementary Table S4). RT-qPCR results showed that hsa_circ_0010467 overexpression or knockdown specifically targeted hsa_circ_0010467 but not

◂**Fig. 1** The transcriptional characterization and clinical significance of hsa_circ_0010467 in OC cells and tissues. **A** Volcano plot showing the differences of circRNAs between samples derived from platinum-resistant (n = 8) and platinum-sensitive (n = 10) OC patients. **B** Information about the exonic structure and Sanger sequencing validation of back-splicing junction of hsa_circ_0010467. **C** RT-qPCR products generated with divergent and convergent primers showing the circularization of hsa_circ_0010467. cDNA, complementary DNA. gDNA, genomic DNA. **D** RT-qPCR analysis of the expression of hsa_circ_0010467 and EIF4G3 mRNA in A2780-DDP/SKOV3-DDP cells after treatment with RNase R. **E** FISH analysis of hsa_circ_0010467. Nuclei are stained with DAPI. **F** Nucleocytoplasmic fractionation experiment showing the distribution of hsa_circ_0010467 in cytoplasm and nucleus. **G** The RT-qPCR quantification of hsa_circ_0010467 expression level in OC cell lines and platinum-resistant OC cell lines. **H** RT-qPCR analysis of hsa_circ_0010467 and EIF4G3 mRNA expression levels in A2780/SKOV3 and A2780-DDP/SKOV3-DDP cells. **I** Comparison of hsa_circ_0010467 levels between platinum-resistant (n = 30) and platinum-sensitive (n = 37) OC tissues. **J** Kaplan–Meier analysis of the association between hsa_circ_0010467 levels and overall survival of 110 OC patients. Expression levels of hsa_circ_0010467 are divided into high and low subgroups according to the median relative RNA abundance. **K** Association analysis between hsa_circ_0010467 levels and tumor stages. **L** RT-qPCR analysis of hsa_circ_0010467 expression in the primary tumor tissues of 7 OC patients with platinum-resistant relapse and 7 OC patients with platinum-sensitive relapse. **M** RT-qPCR analysis of hsa_circ_0010467 levels in plasma EVs of platinum-resistant (n = 21) and platinum-sensitive (n = 12) OC patients. The data are presented as the means ± SEM of at least three independent experiments. *P < 0.05, **P < 0.01, ***P < 0.001, ****P < 0.0001

EIF4G3 mRNA in A2780-DDP, SKOV3-DDP, and parental cell lines transfected with the hsa_circ_0010467 overexpression or RNAi vectors (Fig. 2B and C). Knockdown of hsa_circ_0010467 notably suppressed the proliferation ability of A2780-DDP, SKOV3-DDP, and SKOV3 cells (Fig. 2D and Supplementary Figure S4A), whereas overexpression of hsa_circ_0010467 led to an increase of cell proliferation (Fig. 2E and Supplementary Figure S4B). Our EdU assays further demonstrated that hsa_circ_0010467 promoted the cell proliferative ability of OC cells (Supplementary Figure S4C-F).

It has been well known that the cancer stem cells (CSCs) is one of the major factors that decrease the sensitivity of cancer cells to the chemotherapeutic drug cisplatin [31, 32]. To further explore how hsa_circ_0010467 affects platinum resistance of OC patients, we then investigated the effect of hsa_circ_0010467 on ovarian CSCs. We found that hsa_circ_0010467 depletion in A2780-DDP, SKOV3-DDP, and SKOV3 cells significantly decreased the ability of spheroid formation (Fig. 2F). In addition, hsa_circ_0010467 overexpression could rescue the number of spheroids (Fig. 2G). Moreover, the downregulation of hsa_circ_0010467 decreased the expression of ALDH1A, OCT4 and SOX2 (Fig. 2H and Supplementary Figure S4G), which were associated with ovarian CSCs signatures [33–35], whereas these markers were increased upon hsa_circ_0010467 overexpression (Fig. 2I and Supplementary Figure S4H). We further determined the percentage of aldehyde dehydrogenase 1 (ALDH-1)-positive cells, a hallmark of stem cells, between A2780-DDP cells expressing control and PLCDH-hsa_circ_0010467 by fluorescence-activated cell sorting. Hsa_circ_0010467 overexpression was found to significantly increase ALDH-positive cells from 38.3% to 75.5% in A2780-DDP cells (Fig. 2J and Supplementary Figure S4I). In addition, the sihsa_circ_0010467-1 and sihsa_circ_0010467-2 were transfected into A2780-DDP and SKOV3-DDP cells, which showed no effect on the expression of EIF4G3 (Supplementary Figure S5A). Further colony formation, CCK8, EdU, and spheroid formation assays demonstrated that hsa_circ_0010467 knockdown inhibited the proliferation and CSC self-renewal ability of A2780-DDP and SKOV3-DDP cells (Supplementary Figure S5B-E). Altogether, these results indicated that hsa_circ_0010467 was required to maintain cell viability and CSC population in OC.

Hsa_circ_0010467 regulates the sensitivity of OC cells to cisplatin

To further clarify the function of hsa_circ_0010467 in cisplatin resistance, we overexpressed hsa_circ_0010467 in OC cisplatin-resistant cell lines with a hsa_circ_0010467 plasmid or silenced hsa_circ_0010467 with two shRNAs or two siRNAs without altering EIF4G3 expression. The upregulation of hsa_circ_0010467 increased the half-maximal inhibitory concentration (IC50) of cisplatin in A2780-DDP and SKOV3-DDP cells (Fig. 3A). Conversely, silencing hsa_circ_0010467 abrogated hsa_circ_0010467-induced cisplatin resistance in OC cisplatin-resistant cell lines (Fig. 3B and Supplementary Figure S5F). Colony formation assays showed that hsa_circ_0010467-silencing cells had a lower survival rate than the control after exposure to cisplatin (Fig. 3C and D). To further examine the critical role of hsa_circ_0010467 in platinum resistance, tumor ascite samples obtained from consenting platinum-resistant OC patients who underwent drainage of ascites effusion (Supplementary Table S5). Platinum-resistant OC PDOs were successfully established from appropriate OC tissues. Briefly, these tissues were suspended in basement membrane extract (BME), plated and supplemented with medium for organoid derivation (Fig. 3E). To compare these organoids to their corresponding tumor tissue, we performed hematoxylin and eosin (H&E) staining and evaluated expression of OC protein biomarkers, such as paired box gene 8 (PAX8) [26, 36]. Histological comparison of HGSOC organoids and their corresponding tumors showed that PAX8 positively stained both organoids and the tumor cells within the tissue (Supplementary Figure S6A). The OC organoids were infected with lentiviruses

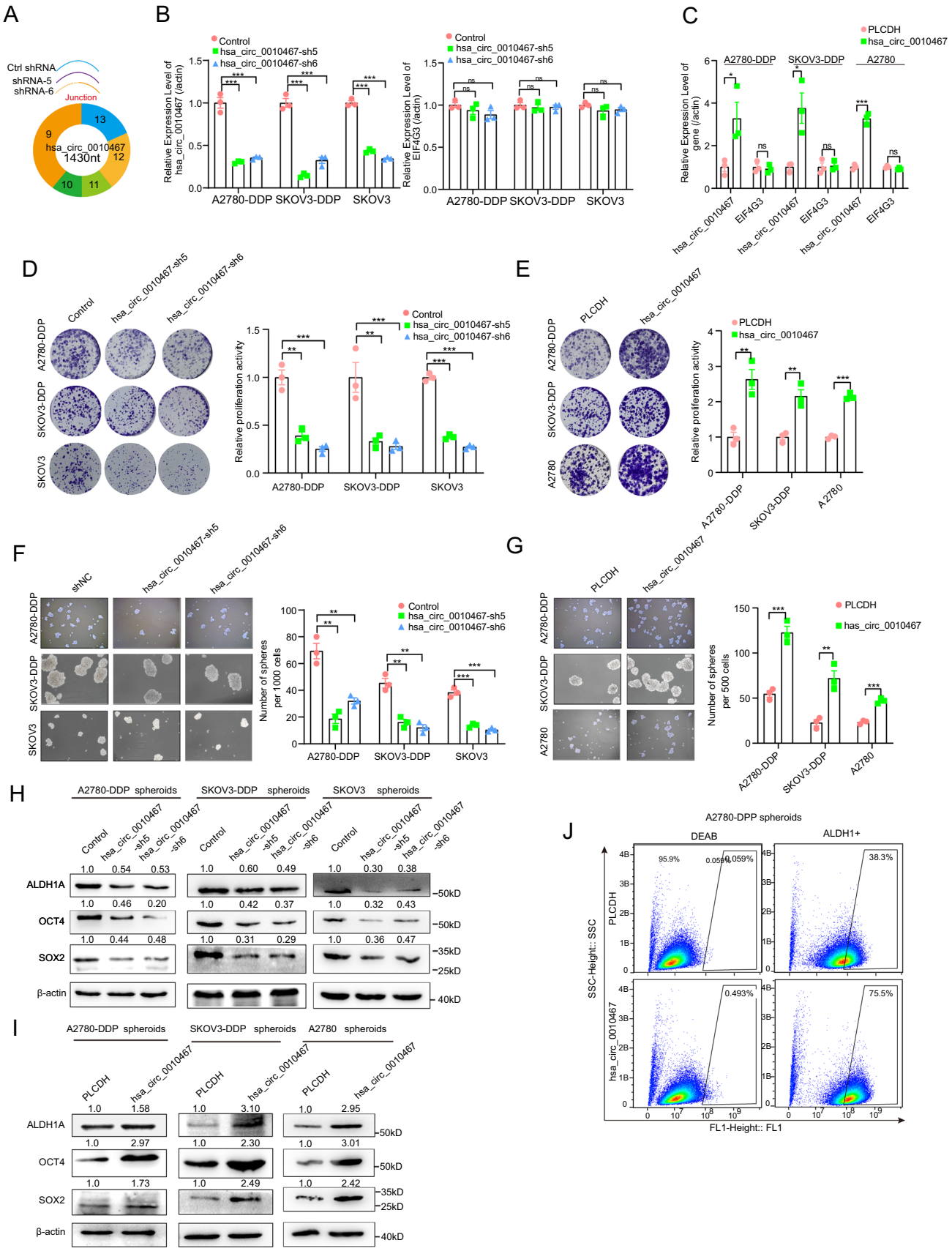
A
Ctrl shRNA
shRNA-5
shRNA-6
Junction
hsa_circ_0010467
1430nt
B
Control
hsa_circ_0010467-sh5
hsa_circ_0010467-sh6
Relative Expression Level of hsa_circ_0010467 (/actin)
Relative Expression Level of EIF4G3 (/actin)
A2780-DDP SKOV3-DDP SKOV3
C
PLCDH
hsa_circ_0010467
A2780-DDP SKOV3-DDP A2780
Relative Expression Level of gene (/actin)
hsa_circ_0010467 EIF4G3
D
Relative proliferation activity
E
F
shNC
Number of spheres per 1000 cells
G
Number of spheres per 500 cells
H
A2780-DDP spheroids SKOV3-DDP spheroids SKOV3 spheroids
ALDH1A
OCT4
SOX2
β-actin
I
J
A2780-DPP spheroids
DEAB
ALDH1+
SSC-Height:: SSC
FL1-Height:: FL1

◂**Fig. 2** Hsa_circ_0010467 promotes the proliferation of OC cells and OC CSC self-renewal maintenance. **A** The construction of two different shRNAs that target the hsa_circ_0010467 junction site. **B** The expression of hsa_circ_0010467 and EIF4G3 mRNA in A2780-DDP/SKOV3-DDP/SKOV3 cells are analyzed by RT-qPCR after transfection with the two shRNAs or the control shRNA. (**C**) The levels of hsa_circ_0010467 and EIF4G3 mRNA in A2780-DDP/SKOV3-DDP/A2780 cells are analyzed by RT-qPCR after stable transfection with the hsa_circ_0010467 overexpression vector (hsa_circ_0010467) or the control vector (pLCDH). **D** Downregulation of hsa_circ_0010467 significantly inhibits the proliferation of A2780-DDP/SKOV3-DDP/SKOV3 cells. **E** Ectopic upregulation of hsa_circ_0010467 promotes the proliferation of A2780-DDP/SKOV3-DDP/A2780 cells. **F** Knockdown of hsa_circ_0010467 decreases the capacity of spheroid formation in A2780-DDP/SKOV3-DDP/SKOV3 cells. **G** Overexpression of hsa_circ_0010467 rescues the spheroid formation reduced by hsa_circ_0010467 knockdown. **H** Hsa_circ_0010467 knockdown decreases the expression of CSC markers in protein levels. **I** Overexpression of hsa_circ_0010467 rescues the expression of CSC markers in protein levels that are reduced by hsa_circ_0010467 knockdown. The proteins of ALDH1A, OCT4, and SOX2 are isolated from spheroids for Western blotting. **J** Representative FACS analysis showing the $ALDH1^+$ cell populations in hsa_circ_0010467 overexpression and control A2780-DDP cells. The data are presented as the means ± SEM of at least three independent experiments. *P < 0.05, **P < 0.01, ***P < 0.001, ****P < 0.0001

carrying shRNAs targeting hsa_circ_0010467 to achieve specific knockdown (Supplementary Figure S6B). We also use a lentivirus vector with GFP (pLV3-U6-MCS-shRNA-EF1a-CopGFP-Puro) (P29436, Miaoling Biology, Wuhan) to verify the successful establishment of the knockdown system (Supplementary Figure S6C). Upon cisplatin treatment, fewer organoids formed in the hsa_circ_0010467 knockdown group than that in the control (Fig. 3F and Supplementary Figure S6D), and their sizes were much smaller as well (Supplementary Figure S6E). Next, we further confirmed the role of hsa_circ_0010467 in cisplatin resistance in ovarian xenograft tumor models (Supplementary Figure S6F). A2780-DDP cells were subcutaneously injected into the dorsal flank of nude mice with or without knockdown hsa_circ_0010467. When the tumor diameter reached 3 mm, the mice received 5 treatments of intraperitoneal injection of 5 mg/kg cisplatin or PBS. Our results showed that silencing hsa_circ_0010467 could inhibit tumor growth, as demonstrated by the size and weight of tumors in the knockdown group compared with those in the control group, and the hsa_circ_0010467-sh6 + cisplatin group showed the highest antitumor capability (Fig. 3G, H and I). We also found that the number of apoptotic cells significantly increased, while that of Ki67-positive cells decreased in mice treated with control + cisplatin, hsa_circ_0010467-sh6 + GS or hsa_circ_0010467-sh6 + cisplatin alone (Supplementary Figure S6G). This observation was more obvious in the hsa_circ_0010467-sh6 + cisplatin group than in the hsa_circ_0010467-sh6 + GS or control + cisplatin group (Supplementary Figure S6G), indicating the synergistic antitumor capability of hsa_circ_0010467-sh6 and cisplatin. Our results showed that hsa_circ_0010467 was essential for sustaining cisplatin resistance and that silencing hsa_circ_0010467 substantially increased the anti-tumor efficacy of cisplatin by reducing tumor cell proliferation.

Hsa_circ_0010467 enhances the activation of STAT3

To further investigate how hsa_circ_0010467 exerted its function in sustaining cisplatin resistance, we performed RNA-seq following hsa_circ_0010467 knockdown to detect gene expression changes in A2780-DDP cells. Integrative gene set enrichment analysis (GSEA) of RNA-seq data was then conducted. We noticed that several genes in oncogenic signaling pathways, including MYC, JAK/STAT3, TNFα/NF-κB, and E2F, were remarkably suppressed with hsa_circ_0010467 depletion (Fig. 4A and B). Our analysis also revealed the significant enrichment of pluripotency of stem cell, TNF, TGF-beta, and Hippo signaling pathways in hsa_circ_0010467-silencing A2780-DDP cells (Fig. 4C). JAK/STAT3 had been found to regulate cancer stemness [37–39], which also played an important role in sustaining drug resistance. Therefore, we focused on altered genes in the JAK/STAT3 signaling pathway. The mRNA levels of the STAT3 downstream effectors were further examined by RT-qPCR analyses, after the transfection of hsa_circ_0010467 siRNA or siNC, or infection by lentivirus PLCDH-hsa_circ_0010467 or PLCDH-Vector in A2780-DDP/SKOV3-DDP cells. The results showed that LIF was the most significantly downregulated gene in hsa_circ_0010467-silencing cells (Fig. 4D). The transcription factor STAT3 was the primary signaling molecule in the JAK/STAT3 pathway, and the activation of STAT3 was associated with CSCs [37]. The knockdown of hsa_circ_0010467 drastically reduced the level of phospho-STAT3 (Tyr705) (pSTAT3), but not the whole levels of STAT3, suggesting that hsa_circ_0010467 mediate the phosphorylation and activation of STAT3 (Fig. 4E).

Next, we investigated whether hsa_circ_0010467 affected the cancer stemness. It has been demonstrated that the expression of SOX2, KLF4, OCT4, NANOG, and ALDH1A are associated with OC CSC signatures [39, 40]. Our RNA-seq analysis revealed that hsa_circ_0010467 knockdown affected the expression of KLF4 (Fig. 4F). We further confirmed that hsa_circ_0010467 knockdown reduced the expression of SOX2, KLF4, OCT4, NANOG, and ALDH1A in A2780-DDP/SKOV3-DDP cells (Fig. 4G). Taken together, these findings illustrated that the abnormal expression of hsa_circ_0010467 mediated cancer proliferation and cancer stemness by promoting STAT3 activation.

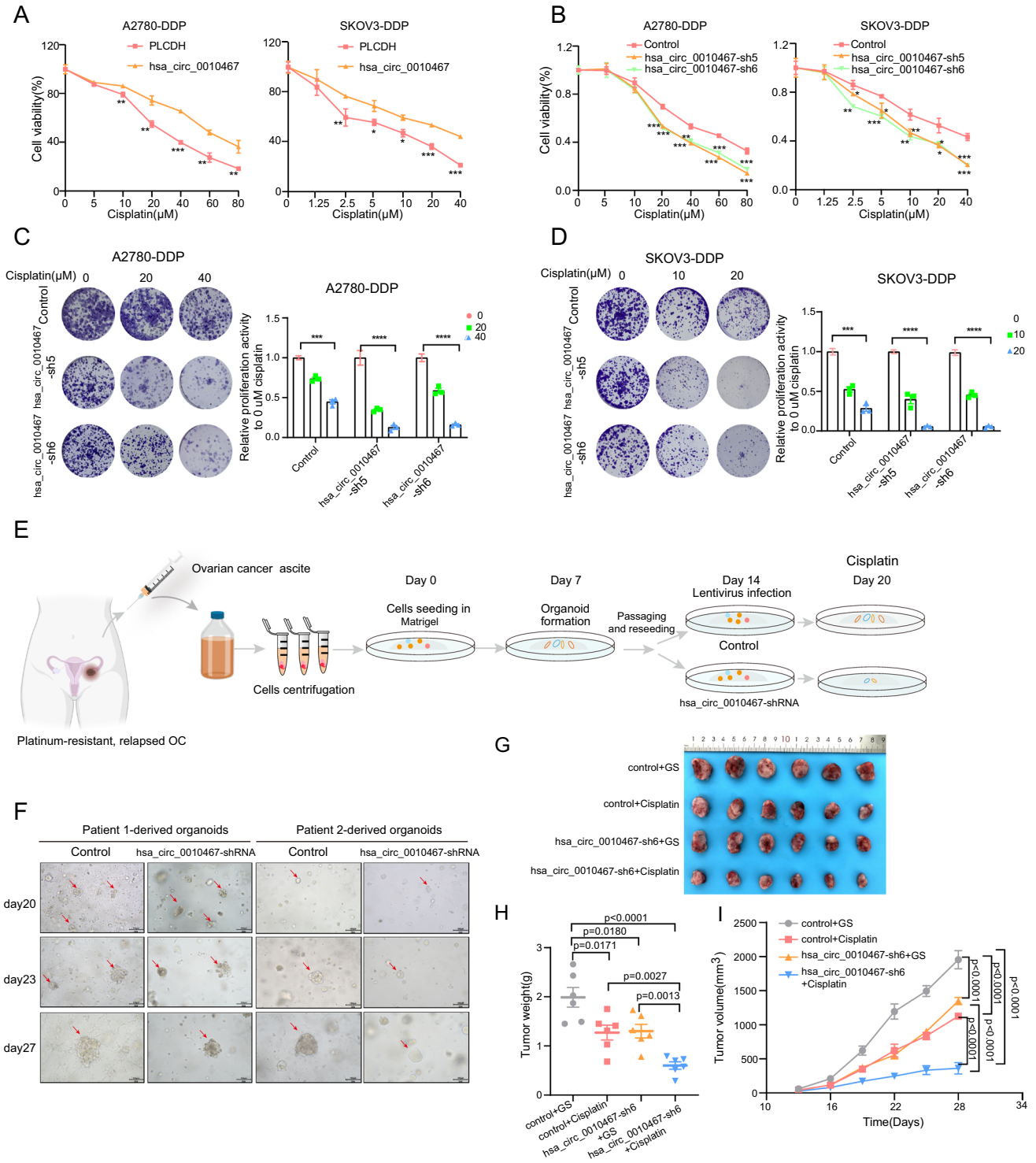

Fig. 3 Hsa_circ_0010467 regulates the sensitivity of OC cells to cisplatin in vivo and in vitro. Stable hsa_circ_0010467 knockdown (**A**) or hsa_circ_0010467 overexpression (**B**) in A2780-DDP and SKOV3-DDP cells that are treated with cisplatin of different concentrations for 48 h, and cell viability is measured by the CCK8 assay. Colony formation assays show that shRNA-mediated depletion of hsa_circ_0010467 leads to cell number changes in response to cisplatin treatment in A2780-DDP (**C**) and SKOV3-DDP cells (**D**) that are treated with different concentrations of cisplatin (0, 20, and 40 μM) or cisplatin (0, 10, and 20 μM) for 2 weeks, and colonies were visualized by crystal violet staining. **E** Schematic illustrating the establishment and subsequent treatments of the platinum-resistant OC patient-derived organoids (PDOs). **F** Downregulation of hsa_circ_0010467 significantly inhibited the proliferation of platinum-resistant OC PDOs. **G** The image of xenograft tumors derived from sacrificed mice in subcutaneous xenograft model. In vivo analysis of tumor weights (**H**) and volumes (**I**) in mice with indicated treatment. n = 6 tumors, two-sided Student's t-test. The data are presented as the mean ± SEM, *P < 0.05, **P < 0.01, ***P < 0.001, ****P < 0.0001

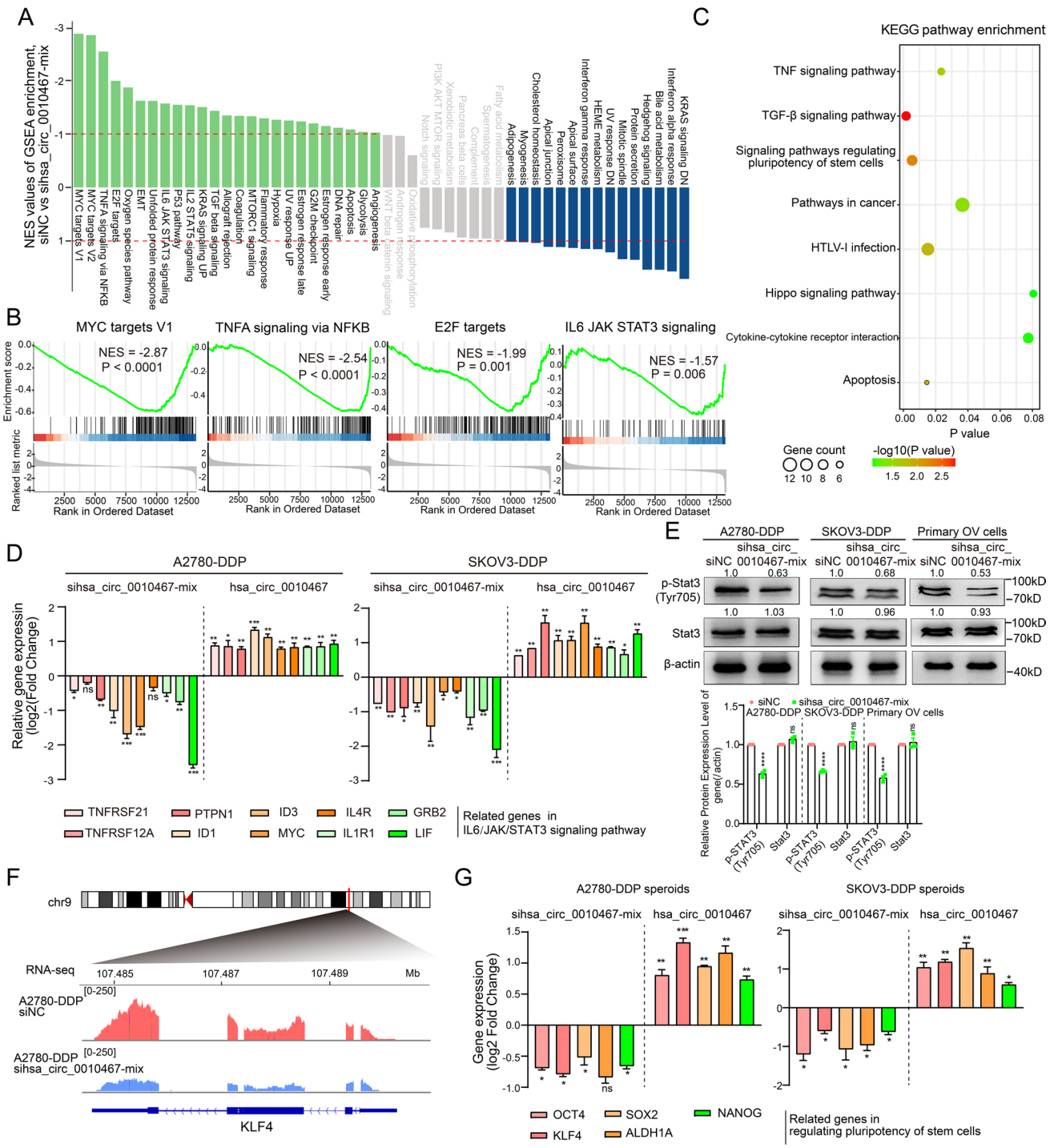

Fig. 4 Hsa_circ_0010467 modulates OC cell proliferation and cancer stemness by promoting IL6/JAK/STAT3 signaling pathway. **A** Bar plots showing enriched GSEA pathways by differentially expressed genes (sihsa_circ_0010467/siNC, absolute fold change > 1.5) in A2780-DDP cells. X-axis indicates GSEA pathways and Y-axis represents statistical significance of the enrichment. **B** GSEA analysis shows that the MYC, JAK/STAT3, TNFα/NF-κB, and E2F signaling pathway related genes were significantly enriched in A2780-DDP cells with hsa_circ_0010467 knockdown. **C** Bubble chart showing the top enriched KEGG pathways of downregulated genes (sihsa_circ_0010467-mix/siNC, fold change > 1.5) in A2780-DDP cells. **D** JAK/STAT3 signaling pathway-related genes are detected by RT-qPCR. **E** Western blot analysis of pSTAT3 and STAT3 in A2780-DDP, SKOV3-DDP, and primary platinum-resistant patients' cells with hsa_circ_0010467 knockdown. The bottom panel showing the statistical analysis of pSTAT3 and STAT3 expression (n = 3). **F** The RNA-seq reads around the KLF4 loci. **G** RT-qPCR analysis of the mRNA expression of SOX2, KLF4, OCT4, NANOG, and ALDH1A in A2780-DDP and SKOV3-DDP spheroids with hsa_circ_0010467 knockdown or overexpression. The data are presented as the means ± SEM of at least three independent experiments. *P < 0.05, **P < 0.01, ***P < 0.001, ****P < 0.0001

Hsa_circ_0010467 directly binds to miR-637 and acts as a competitive endogenous RNA

Given its preferential localization in the cytoplasm and lack of potential open reading frame (ORF), we hypothesized that hsa_circ_0010467 could serve as a miRNA sponge to compete with endogenous RNAs. We screened potential miRNA targets by employing the circbank [41], circAtlas [42], and circinteractome [43] tools, which identified four miRNA candidates, including miR-637, miR-578, miR-767-5p, and miR-892b (Fig. 5A and B). To identify whether these miRNAs could bind to hsa_circ_0010467, biotinylated hsa_circ_0010467 probes targeting the junction site and scrambled oligo probes were designed and applied to perform RNA pull-down assay in A2780-DDP/SKOV3-DDP cells (Fig. 5C). The enrichments of miR-637 in the hsa_circ_0010467 pulldown fraction were significantly higher than those of the other miRNAs (Fig. 5D). Furthermore, RNA immunoprecipitation (RIP) was performed to observe whether hsa_circ_0010467 could bind to miR-637 (Fig. 5E). The RIP results showed higher levels of miR-637 and hsa_circ_0010467 in the Flag antibody group than those in the IgG control group (Fig. 5F). Next, we performed dual-luciferase reporter assays via co-transfecting luciferase reporter vectors psicheck2-hsa_circ_0010467 and miRNA mimics in HEK293T cells. Compared to the negative control group or three miRNAs (miR-578, miR-767-5p and miR-892b), the luciferase activity of hsa_circ_0010467 decreased by 50% in the miR-637 mimics group (Fig. 5G). Moreover, after mutating the binding sites of miR-637 in hsa_circ_0010467 (Fig. 5H), we found that miR-637 did not induce any significant change in luciferase activity of hsa_circ_0010467 Mut (Fig. 5I). Furthermore, we found that miR-637 expression was significantly decreased after hsa_circ_0010467 overexpression, whereas hsa_circ_0010467 knockdown led to increased miR-637 expression in A2780-DDP/SKOV3-DDP cells (Fig. 5J). Pearson correlation analysis revealed that the expression of hsa_circ_0010467 was reversely correlated with the level of miR-637 in OC tissues (Fig. 5K). Together, our results suggested that hsa_circ_0010467 could directly bind to miR-637 and acted as a sponge of miR-637.

LIF is a direct target of miR-637 and stimulates LIF-STAT3 pathway

LIF had been shown to be a target gene of miR-637, which subsequently activated the JAK/STAT3 pathway to promote tumor progression via regulating STAT3 tyrosine 705 phosphorylation [44–47]. To further validate this in platinum resistant OC cells, the miR-637 mimic or miR-637 inhibitor was transfected into A2780-DDP cells. Overexpression of miR-637 decreased the protein and mRNA expression level of LIF, while downregulation of miR-637 increased the protein and mRNA expression level of LIF (Fig. 6A and B). Then, plasmids containing the wild-type sequence (LIF-WT) or the mutant binding site sequence (LIF-Mut) were constructed (Fig. 6C) and co-transfected with the miR-637 mimic or NC mimic into HEK293T cells for a dual luciferase reporter assay. The results showed that overexpression of miR-637 significantly reduced the luciferase activity of the vector containing LIF-WT but did not reduce the luciferase activity of the empty vector or the vector containing LIF-Mut (Fig. 6D). Pearson correlation analysis showed that the expression of LIF was negatively correlated with the level of miR-637 in OC tissues (Fig. 6E). These results demonstrated that LIF was the direct target gene of miR-637.

Subsequently, the expression of LIF was further evaluated in A2780-DDP/SKOV3-DDP cells after knockdown of hsa_circ_0010467. The results showed that downregulation of hsa_circ_0010467 led to a decrease in the expression of LIF (Fig. 6F, G and H). Moreover, knockdown of hsa_circ_0010467 decreased the protein expression level of LIF, inhibiting STAT3 tyrosine 705 phosphorylation (Fig. 6I). In addition, the expression of LIF was examined in OC tissues and normal ovarian tissues by RT-qPCR. It was found that LIF was significantly upregulated in OC tissues compared to normal tissues, and upregulated in resistant OC tissues compared to platinum-sensitive OC tissues (Fig. 6J). Analysis using GEPIA2 [48] (http://gepia2.cancer-pku.cn) showed that LIF was significantly upregulated in tumor tissues compared with normal ovarian tissues in the TCGA OC cohort (Fig. 6K). Pearson correlation analysis showed that the expression of LIF was positively correlated with the level of hsa_circ_0010467 (Fig. 6L) in OC tissues. In summary, these results demonstrated that hsa_circ_0010467 could function as a sponge of miR-637 to activate the LIF/STAT3 pathway.

Hsa_circ_0010467 sustains cisplatin resistance through miR-637/LIF/STAT3

To further investigate whether hsa_circ_0010467 played its biological role via the hsa_circ_0010467/miR-637/LIF/STAT3 axis, a series of rescue experiments were executed in A2780-DDP/SKOV3-DDP cells after co-transfection of miR-637 mimic or miR-637 inhibitor with hsa_circ_0010467 or sihsa_circ_0010467-mix. The results of colony formation, spheroid formation, and EdU assays showed that the miR-637 inhibitor reversed the alteration in the biological behaviors of OC cells induced by hsa_circ_0010467 knockdown (Fig. 7A–D). Conversely, the miR-637 mimic offset the alteration in the biological behaviors of OC cells induced by overexpression of hsa_circ_0010467 (Fig. 7A–D). The downregulation of hsa_circ_0010467 decreased LIF protein expression and the miR-637 inhibitor rescued protein expression, while

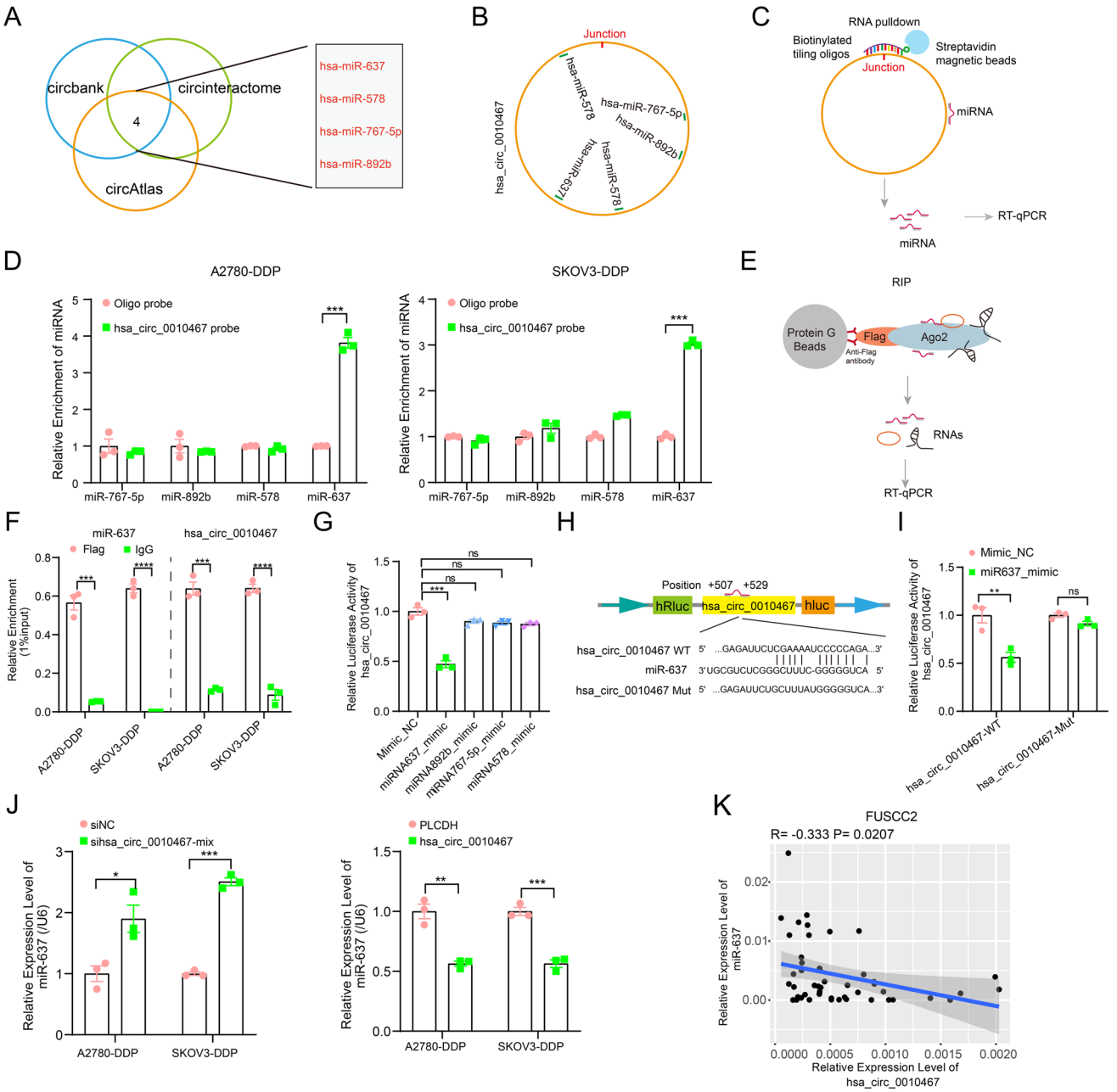

Fig. 5 Hsa_circ_0010467 acts as an miR-637 sponge in OC. **A** The potential target miRNAs of hsa_circ_0010467 are predicted from the circBank, circAlats, and circinteractome databases. **B** Predicted relative positions of target miRNAs on hsa_circ_0010467. **C** Flow chart of RNA pulldown assay design. **D** RT-qPCR is utilized to determine the relative enrichment levels of four potential target miRNAs in precipitates from A2780-DDP and SKOV3-DDP cell lysates pulled down by the hsa_circ_0010467 probe or oligo probe. **E** Flow chart of AGO2-RIP assay design. **F** The RIP assays are performed using a flag antibody against AGO2-flag with extracts from A2780-DDP and SKOV3-DDP cells. Enrichment of miR-637 and hsa_circ_0010467 in RNA samples after RIP assays is determined by RT-qPCR analysis. **G** The four miRNAs are validated through a luciferase reporter gene assay. **H** A schematic diagram showing the binding site of miR-637. **I** Hsa_circ_0010467-WT or hsa_circ_0010467-Mut and miR-637 mimics were co-transfected into HEK293T cells, and a luciferase reporter gene assay is utilized to evaluate luciferase activity. **J** Expression of miR-637 in A2780-DDP/SKOV3-DDP cells with hsa_circ_0010467 knockdown or overexpression is determined by RT-qPCR analysis. **K** The expression correlation between hsa_circ_0010467 and miR-637 in the FUSCC2 OC cohort. The data are presented as the means ± SEM of at least three independent experiments. *P < 0.05, **P < 0.01, ***P < 0.001, ****P < 0.0001

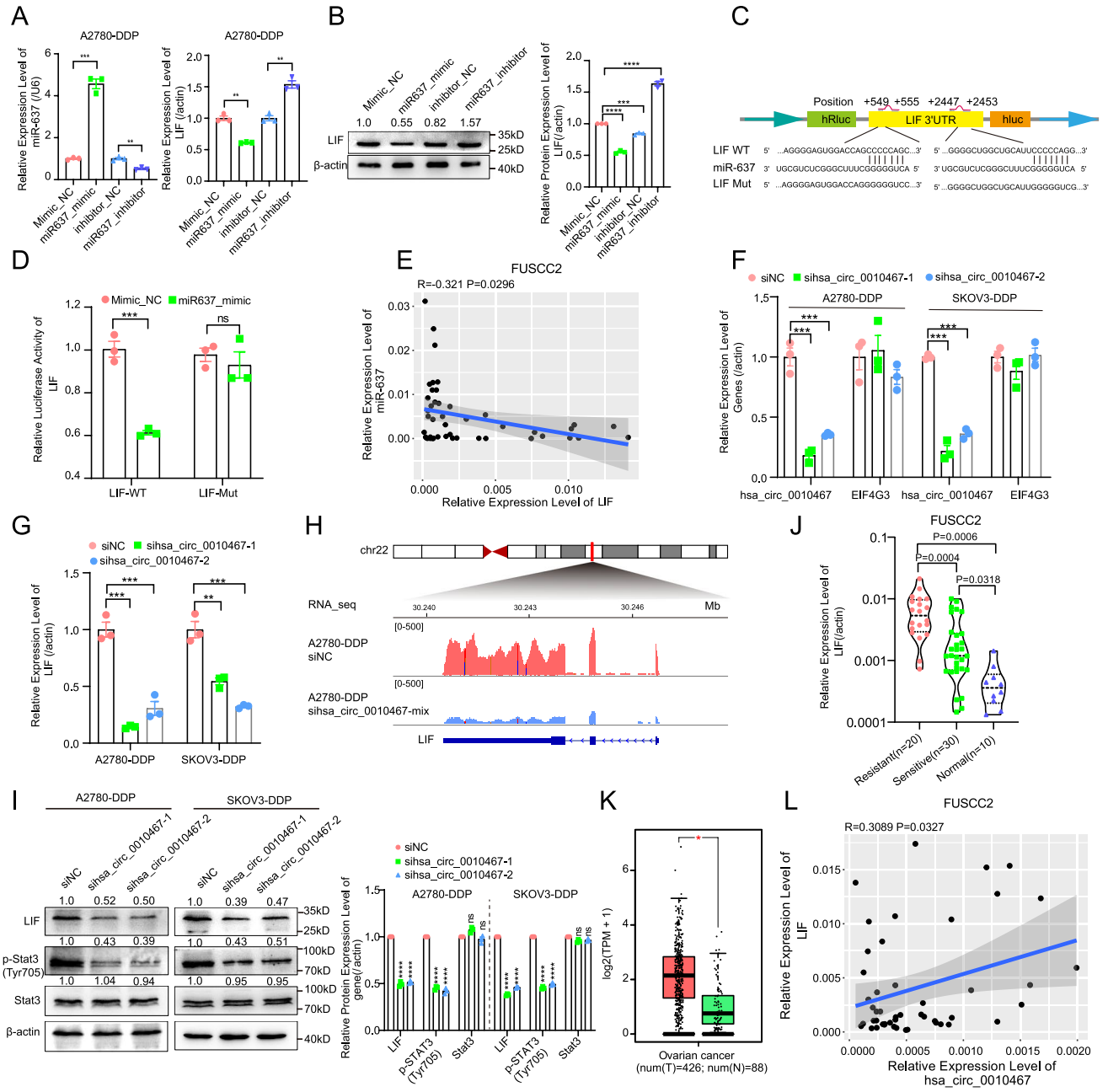

Fig. 6 Hsa_circ_0010467 elevates LIF expression and stimulates LIF-STAT3 pathway by sponging miR-637 in OC. **A** The relative mRNA expression of LIF after transfection with miR-637 mimic, miR-637 inhibitor, or control. **B** The protein expression of LIF after transfection with miR-637 mimic, miR-637 inhibitor or control. The right panel showing the statistical analysis of LIF expression (n = 3). **C** A schematic diagram showing the binding sites of miR-637 in LIF 3′ UTR. **D** LIF-WT or LIF-Mut and miR-637 mimics were co-transfected into HEK293T cells, and a luciferase reporter gene assay is utilized to evaluate luciferase activity. **E** Pearson correlation analysis of LIF and miR-637 expression in OC tissues. **F** The relative expression of hsa_circ_0010467 and EIF4G3 in A2780-DDP and SKOV3-DDP cell lines with hsa_circ_0010467 knockdown or control. **G** RT-qPCR results showing the relative expression of LIF after silencing hsa_circ_0010467. **H** The RNA-seq reads around the LIF loci, and a significantly downregulated peak is observed after hsa_circ_0010467 knockdown. **I** Western blot results showing the relative protein levels of LIF and downstream LIF-STAT3 pathway-related molecules are measured in A2780-DDP and SKOV3-DDP cells after silencing hsa_circ_0010467. The right panel showing the statistical analysis of LIF, pSTAT3, and STAT3 expression (n = 3). **J** RT-qPCR results showing the relative expression of LIF in the platinum-resistant, platinum-sensitive OC tissues, and normal ovarian tissues. **K** LIF is significantly upregulated in the TCGA ovarian cancer cohort. **L** The expression correlation between LIF and hsa_circ_0010467 in the FUSCC2 OC cohort. The data are presented as the means ± SEM of at least three independent experiments. *P < 0.05, **P < 0.01, ***P < 0.001, ****P < 0.0001

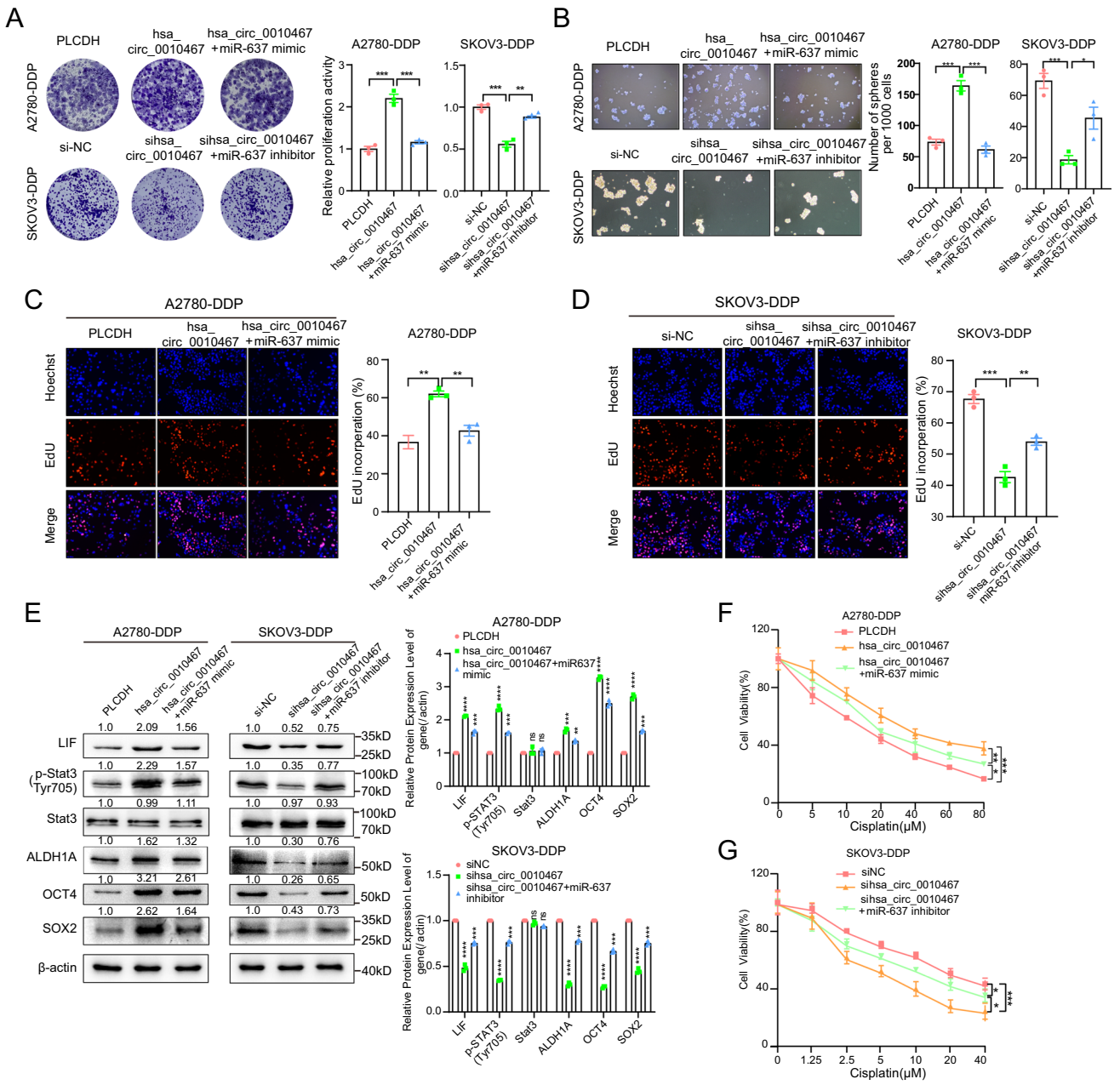

Fig. 7 Hsa_circ_0010467 sustains cisplatin resistance and CSC self-renewal ability through miR-637/LIF. The cell viability and spherois formation capacity of A2780-DDP/SKOV3-DDP cells are detected after transfection or co-transfection with indicated vectors, siRNAs, miRNAs or inhibitors by colony formation assays (**A**), spheroid formation assays (**B**), and EdU assays (**C** and **D**), respectively. **E** The relative protein levels of LIF and downstream LIF/STAT3 pathway-related molecules that are measured in A2780-DDP/SKOV3-DDP cells after transfection or co-transfection with indicated vectors, siRNAs, miRNA mimics or inhibitors by Western blot. The right panel showing the statistical analysis for protein expression of LIF, pSTAT3, STAT3, ALDH1A, OCT4, and SOX2 in A2780-DDP/SKOV3-DDP cells (n = 3). **F** A2780-DDP cells transfected with PLCDH, hsa_circ_0010467, or hsa_circ_0010467 + miR-637 mimic are treated with cisplatin at different concentrations for 48 h, and cell viability is measured by CCK8 assays. **G** SKOV3-DDP cells transfected with siNC, sihsa_circ_0010467, or sihsa_circ_0010467 + miR-637 inhibitor are treated with different concentrations of cisplatin for 48 h, and cell viability is evaluated by CCK-8 assays. The data are presented as the means ± SEM of at least three independent experiments. *P < 0.05, **P < 0.01, ***P < 0.001, ****P < 0.0001

upregulation of hsa_circ_0010467 and transfection with the miR-637 mimic caused the opposite effects (Fig. 7E and Supplementary Figure S7A). Additionally, western blot analysis also confirmed that the miR-637 inhibitor and mimic reversed the alterations in cancer stemness-related protein levels caused by hsa_circ_0010467 silencing or overexpression (Fig. 7E and Supplementary Figure S7A).

To further determine whether hsa_circ_0010467 regulated the chemosensitivity of OC through the hsa_circ_0010467/miR-637/LIF/STAT3 axis, a series of gain-of-function assays were conducted. After co-transfection of miR-637 mimic or miR-637 inhibitor with hsa_circ_0010467 or sihsa_circ_0010467-mix, cisplatin was used for the treatment of the A2780-DDP/SKOV3-DDP cells. The effects of the hsa_circ_0010467 on proliferation were reversed by co-transfection with the miR-637 mimic or miR-637 inhibitor (Supplementary Figure S7B-E). The result of drug sensitivity assays also confirmed that miR-637 mimic reversed the promotion in the cisplatin resistance of OC cells caused by hsa_circ_0010467 overexpression, and miR-637 inhibitor offset the promotion in cisplatin-sensitive OC cells induced by hsa_circ_0010467 knockdown (Fig. 7F, G and Supplementary Figure S7F, S7G). Moreover, colony formation and spheroid formation assays also confirmed that LIF overexpression offset the inhibition in the biological behaviors of OC cells induced by hsa_circ_0010467 knockdown (Supplementary Figure S8A-C). Cryptotanshinone is an inhibitor of JAK/STAT3 and significantly inhibits the STAT3 Tyr705 phosphorylation and the dimerization of STAT3 [49, 50]. We used cryptotanshinone to treat OC cells with hsa_circ_0010467 overexpression. The expression level of STAT3 Tyr705 phosphorylation was reduced and verified by western blot analysis (Supplementary Figure S8D). Colony formation and spheroid formation assays also confirmed that cryptotanshinone reversed the promotion in the proliferation ability of OC cells caused by hsa_circ_0010467 overexpression (Supplementary Figure S8E and S8F). Colivelin is a brain penetrant neuroprotective peptide and a potent activator of STAT3, suppresses neuronal death by activating STAT3 in vitro [51, 52]. We used colivelin to treat OC cells with hsa_circ_0010467 knockdown. The expression level of STAT3 Tyr705 phosphorylation was increased and verified by western blot analysis (Supplementary Figure S8G). Colony formation and spheroid formation assays also confirmed that colivelin offset the inhibition in the biological behaviors of OC cells induced by hsa_circ_0010467 knockdown (Supplementary Figure S8H and S8I). Conclusively, hsa_circ_0010467 was demonstrated to sustain cisplatin resistance in OC cells by acting as a ceRNA, which indirectly upregulated the expression of miR-637, LIF, and activated the LIF/STAT3 pathway.

AUF1 mediates the generation of hsa_circ_0010467

We further sought to define the molecular mechanism underlying driving hsa_circ_0010467 up-regulation in platinum-resistant OC. To this end, we first used the online tool circinteractome (https://circinteractome.nia.nih.gov) to identify splicing-associated factors that bind to flanking regions of hsa_circ_0010467. The results suggested that two candidate RNA binding proteins, AUF1 and EIF4A3, contribute to hsa_circ_0010467 cyclization (Fig. 8A). We observed that the expression of hsa_circ_0010467 was significantly down-regulated when AUF1 but not EIF4A3 was silenced (Fig. 8B). Both RIP assay using AUF1 antibody and RT-qPCR analysis indicated that AUF1 protein bound hsa_circ_0010467 (Fig. 8C and D). Notably, AUF1 protein expression was significantly increased in platinum-resistant OC tissues (Fig. 8E). Pearson correlation analysis showed that the expression of AUF1 was positively correlated with that of hsa_circ_0010467 in OC tissues (Fig. 8E). Recently, AUF1 had been reported to regulate circMALAT1 biogenesis and was upregulated in liver cancer stem cells, which contributed to the maintenance of liver cancer stem cells [53]. Then, we isolated patient-derived primary tumor cells (PDC) from platinum-resistant patients' ascites and obtained spheroids by suspension culture. Interestingly, both hsa_circ_0010467 mRNA expression and AUF1 protein expression were significantly increased in spheroids (Fig. 8F and Supplementary Figure S9A). When AUF1 was knocked down in OC cells by two shRNAs, the ability of spheroid formation of OC cells was inhibited (Supplementary Figure S9B). Furthermore, we had successfully constructed PDOs with AUF1 knockdown, and fewer organoids formed in the AUF1 knockdown group than that in the control, and their sizes were much smaller as well (Supplementary Figure S9C and S9D). In summary, these data indicated that the mechanism of hsa_circ_0010467 mediated by AUF1 to promote cancer stemness and cisplatin resistance of OC through hsa_circ_0010467/miR-637/LIF/STAT3 axis (Fig. 8G).

Discussion

Although numerous improved management strategies are available in clinical practice, cancer-related mortality rate of OC remains high, which is largely due to platinum resistance that is a formidable challenge in OC therapy. With the development of high-throughput sequencing techniques, a significant portion of circRNAs that are closely related to tumor resistance have been identified. For instance, upregulation of circFARP1 in cancer-associated fibroblasts contributed to tumor cell stemness, gemcitabine resistance, and ultimately leads to poor survival of pancreatic cancer patients [44]. In vivo experiments demonstrated that silencing circPARD3 inhibited tumorigenicity and enhanced chemosensitivity of laryngeal squamous cell carcinoma cells by enhancing autophagy [54]. Overexpression of circPRKAR1B suppresses the sensitivity of osteosarcoma cells to cisplatin through sponging miR-361-3p to modulate the expression of frizzled class receptor 4 (FZD4) [55]. However, few studies have investigated the role of circRNAs in platinum-resistant OC. In the present study, we found that hsa_circ_0010467

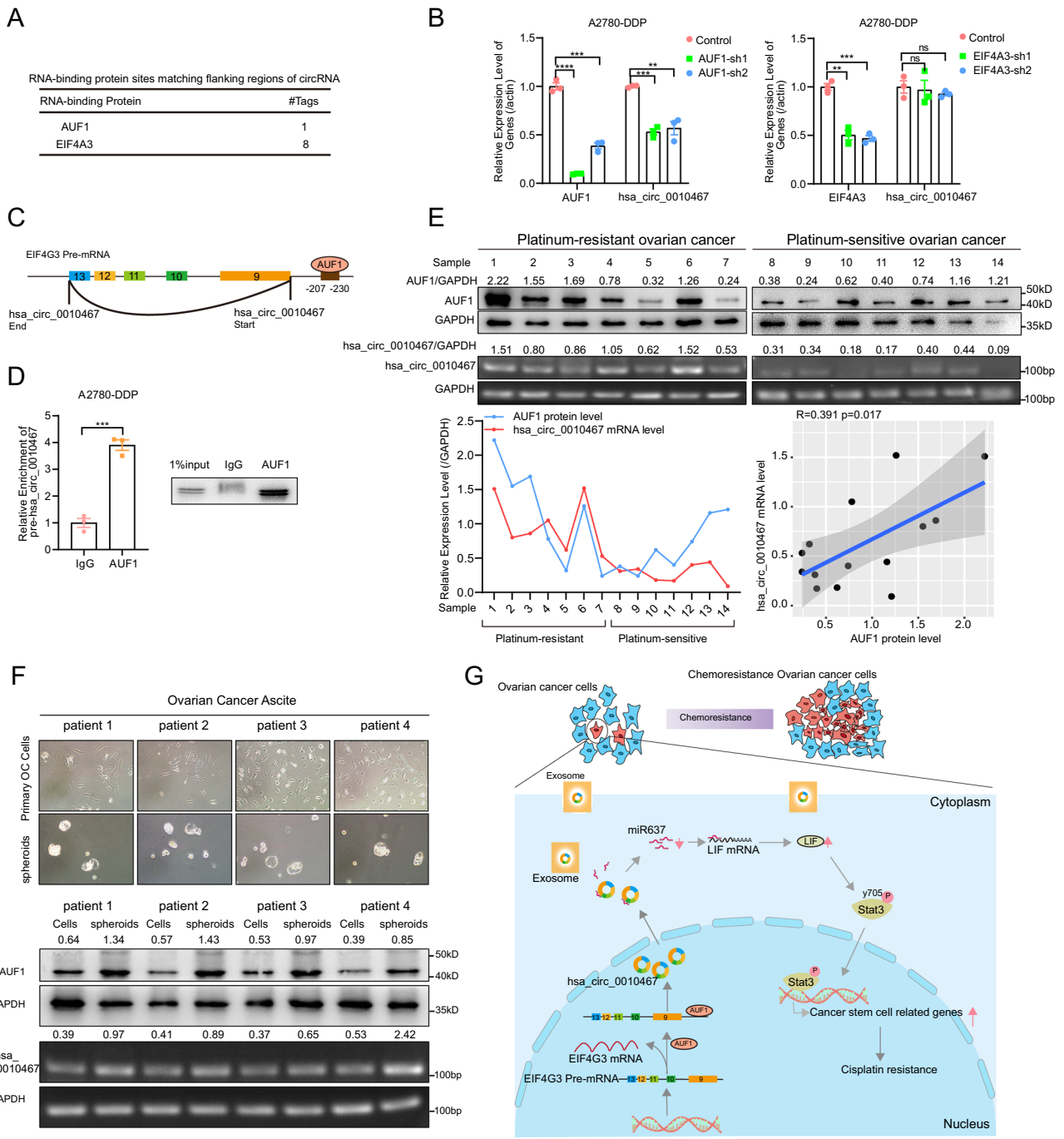

Fig. 8 AUF1 increases hsa_circ_0010467 expression via direct promotion of hsa_circ_0010467 cyclization. **A** Two RNA binding proteins (AUF1 and EIF4A3) were predicted with the circInteractome database. **B** Hsa_circ_0010467 expression is downregulated upon silencing AUF1 (not EIF4A3). **C** The binding sites of AUF1 in the upstream region of the hsa_circ_0010467 pre-mRNA is predicted with the circInteractome database. **D** RIP assay is performed using A2780-DDP cells lysate, either anti-AUF1 or IgG as IP antibody. **E** AUF1 protein expression level and hsa_circ_0010467 mRNA expression level in platinum-resistant (n = 7) and platinum-sensitive OC tissues (n = 7). Line charts below showing the positive correlation between AUF1 and hsa_circ_0010467 expression in OC tissues. **F** AUF1 protein expression level and hsa_circ_0010467 mRNA expression level are detected in primary OC cells and spheroids by Western blot. **G** A schematic diagram illustrates the mechanism how AUF1-induced hsa_circ_0010467 mediated cancer stemness and cisplatin resistance of OC through miR-637/LIF/STAT3 axis. The data are presented as the means ± SEM of at least three independent experiments. *P < 0.05, **P < 0.01, ***P < 0.001, ****P < 0.0001

was highly expressed in platinum-resistant OC tissues and a higher expression level of hsa_circ_0010467 was associated with more advanced tumor stage and poor OC patient prognosis. Our experiments in cells, PDOs and mouse models demonstrated that downregulation of hsa_circ_0010467 increases the sensitivity of OC cells to cisplatin.

Our results showed that hsa_circ_0010467 was upregulated in cisplatin-resistant cell lines, while its cognate EIF4G3 mRNA was downregulated. We found that AUF1, an RNA binding protein, participated in the biogenesis of hsa_circ_0010467, and AUF1 was up-regulated in platinum-resistant ovarian cancer, suggesting that transcriptome alterations mediated by abnormal RBPs during cancer activation and progression may give rise to oncogene activation in a way that does not rely on genomic or epigenomic variations. It is possible that EIF4G3 mRNA might be regulated by miRNAs targeting the 3′ UTR of the mRNA [56]. Further research is needed to completely elucidate transcriptional regulation, processing, and turnover of the transcriptional output of this locus. We next explored the molecular mechanism of hsa_circ_0010467 in OC chemotherapeutic resistance. First, candidate miRNAs with sequences complementary to hsa_circ_0010467 were screened through computational analysis, and it was found that miR-637 expression was also negatively regulated by hsa_circ_0010467 in OC tissues. Furthermore, RNA pulldown, RIP and dual luciferase reporter assays proved a direct interaction between hsa_circ_0010467 and miR-637. MiR-637 had been confirmed to be a tumor suppressor in a variety of cancers [45, 57, 58]. Overexpression of miR-637 dramatically inhibited cell growth and induced the apoptosis of hepatocellular carcinoma (HCC) cells [45]. Decreased miR-637 was an unfavorable progression indicator for glioma patients and promoted glioma cell growth, migration and invasion [57]. Wang et al. found that blockage of miR-637 promoted viability, proliferation, migration and invasion capacity of colorectal cancer cells, suggesting miR-637 played a tumor suppressor role in colorectal cancer [58]. Consistently, we found that overexpression of miR-637 mimicked the effect of hsa_circ_0010467 knockdown in cell proliferation, cancer stemness and chemotherapeutic resistance of OC. Moreover, the effects caused by miR-637 could also be counteracted by hsa_circ_0010467 overexpression. It has been well established that miRNAs regulate gene expression by binding to the complementary sequences in 3′ UTRs of target genes. Our data revealed that miR-637 was able to directly target the 3′ UTR of LIF, resulting in the down regulation of LIF at the post-transcriptional level. Moreover, there was a negative correlation between miR-637 and LIF mRNA in OC tissues. Thus, we hypothesized that LIF might be one of the important targets of miR-637, in agreement with a previous study [45], which reported that miR-637 overexpression negatively regulated STAT3 tyrosine 705 phosphorylation by suppressing LIF expression. Recently, STAT3 activation has been found to be frequently correlated with cancer stemness and chemoresistance [37, 38, 59]. In addition to its direct effects, we found that miR-637 also decreased phosphorylation levels of STAT3 tyrosine 705, and subsequently repressed the transcriptional expression of SOX2, KLF4, OCT4, NANOG, and ALDH1A, which were associated with OC CSCs signatures. In this study, we found that STAT3 activation was inhibited by miR-637 that downregulated LIF expression, which upregulated the expression of OC CSCs signatures, thereby induced cancer stemness and chemoresistance. These could also be observed by silencing hsa_circ_0010467. Conversely, these effects induced by miR-637 could also be rescued by hsa_circ_0010467 overexpression. Furthermore, a positive relationship was observed between hsa_circ_0010467 expression and LIF mRNA in OC tissues. Thus, hsa_circ_0010467 promoted OC progression and chemoresistance through modulating the miR-637/LIF/STAT3 axis.

Previous study had identified AUF1 as a core contributor to circMALAT1 formation [53]. In this study, AUF1 can modulate the biogenesis of hsa_circ_0010467 by combining the upstream region of EIF4G3 pre-mRNA. In addition, AUF1 protein expression was up-regulated in platinum-resistant tissues and spheroids, and its protein expression was positively correlated with hsa_circ_0010467 mRNA. Primary cytoreductive surgery (PCS) followed by platinum-based chemotherapy remains the standard treatment for patients with advanced OC, but lacks appropriate biomarkers and targets to deal with platinum resistance. To test whether hsa_circ_0010467 could be used as a chemotherapy predictor, several cohorts of OC patients who received platinum-based treatment were enrolled. Our results showed that hsa_circ_0010467 was highly expressed in platinum-resistance patients' tissues and plasma exosomes, and its high expression correlated with poor survival, which also significantly increased in platinum-resistant relapse but not platinum-sensitive relapse patients. These results revealed that hsa_circ_0010467 was an appropriate prognostic factor for platinum-resistant patients. In summary, our findings suggest that upregulated hsa_circ_0010467 was necessary for the maintenance of platinum resistance, and silencing hsa_circ_0010467 substantially increased the efficacy of platinum-induced cell death. In summary, our study reveals that hsa_circ_0010467 sequesters miR-637 by acting as a miRNA sponge, thereby competitively activating the LIF/STAT3 pathway and inducing platinum resistance. This study also provides evidence that hsa_circ_0010467 could be a promising biomarker for prognostic prediction in OC patients treated with platinum-based chemotherapy.

Supplementary Information The online version contains supplementary material available at https://doi.org/10.1007/s00018-023-04906-5.

Author contributions X.W. and S.L. conceived and supervised the project; Y.W., and Z.F. collected clinical samples; Y.W. and M.X. conducted the experiments; S.L. and W.H. performed the computational analysis; J.W., X. H., Y.W., S.C., F.X., and H.W. interpreted the results; Y.W., S.L., and X.W. wrote the manuscript with comments from all the other authors; All authors read and approved the final version of the manuscript.

Funding This study was supported by the National Natural Science Foundation of China (81972431 and 32100517) and General Project of Natural Science Foundation of Shanghai (21ZR1415000).

Availability of data and material Raw RNA-seq data are deposited in the Gene Expression Omnibus (GEO) database under the accession number of GSE214302. Software and resources used for data analysis and visualization are described in the method section.

Declarations

Conflict of interest The authors declare no potential conflicts of interest.

Ethics approval and consent to participate All animal experiments were approved by the Animal Care Committee of Fudan University, and were performed in accordance with the light of NIH Guidelines for the Care and Use of Laboratory Animals. The Ethics Committee of Fudan University Shanghai Cancer Center approved the study, and all participants signed informed consent statements.

Consent for publication All authors give consent for the publication of this manuscript.

References

1. Momenimovahed Z, Tiznobaik A, Taheri S, Salehiniya H (2019) Ovarian cancer in the world: epidemiology and risk factors. Int J Womens Health 11:287–299
2. Budiana ING, Angelina M, Pemayun TGA (2019) Ovarian cancer: Pathogenesis and current recommendations for prophylactic surgery. J Turk Ger Gynecol Assoc 20(1):47–54
3. Matulonis UA, Sood AK, Fallowfield L, Howitt BE, Sehouli J, Karlan BY (2016) Ovarian cancer. Nat Rev Dis Primers 2:16061
4. Jeck WR, Sharpless NE (2014) Detecting and characterizing circular RNAs. Nat Biotechnol 32(5):453–461
5. Li S, Han L (2019) Circular RNAs as promising biomarkers in cancer: detection, function, and beyond. Genome Med 11(1):15
6. Fang Z, Jiang C, Li S (2020) The potential regulatory roles of circular RNAs in tumor immunology and immunotherapy. Front Immunol 11:617583
7. Ruan H, Xiang Y, Ko J, Li S, Jing Y, Zhu X, Ye Y, Zhang Z, Mills T, Feng J et al (2019) Comprehensive characterization of circular RNAs in ~ 1000 human cancer cell lines. Genome Med 11(1):55
8. Liang WC, Wong CW, Liang PP, Shi M, Cao Y, Rao ST, Tsui SK, Waye MM, Zhang Q, Fu WM et al (2019) Translation of the circular RNA circbeta-catenin promotes liver cancer cell growth through activation of the Wnt pathway. Genome Biol 20(1):84
9. Sheng R, Li X, Wang Z, Wang X (2020) Circular RNAs and their emerging roles as diagnostic and prognostic biomarkers in ovarian cancer. Cancer Lett 473:139–147
10. Gan X, Zhu H, Jiang X, Obiegbusi SC, Yong M, Long X, Hu J (2020) CircMUC16 promotes autophagy of epithelial ovarian cancer via interaction with ATG13 and miR-199a. Mol Cancer 19(1):45
11. Zhang L, Zhou Q, Qiu Q, Hou L, Wu M, Li J, Li X, Lu B, Cheng X, Liu P et al (2019) CircPLEKHM3 acts as a tumor suppressor through regulation of the miR-9/BRCA1/DNAJB6/KLF4/AKT1 axis in ovarian cancer. Mol Cancer 18(1):144
12. Zhao Z, Ji M, Wang Q, He N, Li Y (2019) Circular RNA Cdr1as upregulates SCAI to suppress cisplatin resistance in ovarian cancer via miR-1270 suppression. Mol Ther Nucleic Acids 18:24–33
13. Li Z, Zhang J, Liu X, Li S, Wang Q, Di C, Hu Z, Yu T, Ding J, Li J et al (2018) The LINC01138 drives malignancies via activating arginine methyltransferase 5 in hepatocellular carcinoma. Nat Commun 9(1):1572
14. Bolger AM, Lohse M, Usadel B (2014) Trimmomatic: a flexible trimmer for Illumina sequence data. Bioinformatics 30(15):2114–2120
15. Kim D, Langmead B, Salzberg SL (2015) HISAT: a fast spliced aligner with low memory requirements. Nat Methods 12(4):357–360
16. Li H, Handsaker B, Wysoker A, Fennell T, Ruan J, Homer N, Marth G, Abecasis G, Durbin R (2009) Genome project data processing S: The sequence alignment/Map format and SAMtools. Bioinformatics 25(16):2078–2079
17. Memczak S, Jens M, Elefsinioti A, Torti F, Krueger J, Rybak A, Maier L, Mackowiak SD, Gregersen LH, Munschauer M et al (2013) Circular RNAs are a large class of animal RNAs with regulatory potency. Nature 495(7441):333–338
18. Westholm JO, Miura P, Olson S, Shenker S, Joseph B, Sanfilippo P, Celniker SE, Graveley BR, Lai EC (2014) Genome-wide analysis of drosophila circular RNAs reveals their structural and sequence properties and age-dependent neural accumulation. Cell Rep 9(5):1966–1980
19. Gao Y, Zhang J, Zhao F (2018) Circular RNA identification based on multiple seed matching. Brief Bioinform 19(5):803–810
20. Zhang XO, Wang HB, Zhang Y, Lu X, Chen LL, Yang L (2014) Complementary sequence-mediated exon circularization. Cell 159(1):134–147
21. Quinlan AR, Hall IM (2010) BEDTools: a flexible suite of utilities for comparing genomic features. Bioinformatics 26(6):841–842
22. Love MI, Huber W, Anders S (2014) Moderated estimation of fold change and dispersion for RNA-seq data with DESeq2. Genome Biol 15(12):550
23. Pertea M, Pertea GM, Antonescu CM, Chang TC, Mendell JT, Salzberg SL (2015) StringTie enables improved reconstruction of a transcriptome from RNA-seq reads. Nat Biotechnol 33(3):290–295
24. Wu T, Hu E, Xu S, Chen M, Guo P, Dai Z, Feng T, Zhou L, Tang W, Zhan L et al (2021) clusterProfiler 4.0: a universal enrichment tool for interpreting omics data. Innovation (Camb) 2(3):100141
25. Liberzon A, Birger C, Thorvaldsdottir H, Ghandi M, Mesirov JP, Tamayo P (2015) The molecular signatures database (MSigDB) hallmark gene set collection. Cell Syst 1(6):417–425
26. Kopper O, de Witte CJ, Lohmussaar K, Valle-Inclan JE, Hami N, Kester L, Balgobind AV, Korving J, Proost N, Begthel H et al (2019) An organoid platform for ovarian cancer captures intra- and interpatient heterogeneity. Nat Med 25(5):838–849
27. Glazar P, Papavasileiou P, Rajewsky N (2014) circBase: a database for circular RNAs. RNA 20(11):1666–1670
28. Nabet BY, Qiu Y, Shabason JE, Wu TJ, Yoon T, Kim BC, Benci JL, DeMichele AM, Tchou J, Marcotrigiano J et al (2017) Exosome RNA unshielding couples stromal activation to pattern recognition receptor signaling in cancer. Cell 170(2):352-366e313

29. Kamerkar S, LeBleu VS, Sugimoto H, Yang S, Ruivo CF, Melo SA, Lee JJ, Kalluri R (2017) Exosomes facilitate therapeutic targeting of oncogenic KRAS in pancreatic cancer. Nature 546(7659):498–503
30. Kahlert C, Kalluri R (2013) Exosomes in tumor microenvironment influence cancer progression and metastasis. J Mol Med (Berl) 91(4):431–437
31. Shafee N, Smith CR, Wei S, Kim Y, Mills GB, Hortobagyi GN, Stanbridge EJ, Lee EY (2008) Cancer stem cells contribute to cisplatin resistance in Brca1/p53-mediated mouse mammary tumors. Cancer Res 68(9):3243–3250
32. Zhang Y, Wang Z, Yu J, Shi J, Wang C, Fu W, Chen Z, Yang J (2012) Cancer stem-like cells contribute to cisplatin resistance and progression in bladder cancer. Cancer Lett 322(1):70–77
33. Wen Y, Hou Y, Yi X, Sun S, Guo J, He X, Li T, Cai J, Wang Z (2021) EZH2 activates CHK1 signaling to promote ovarian cancer chemoresistance by maintaining the properties of cancer stem cells. Theranostics 11(4):1795–1813
34. Yokoyama Y, Zhu H, Lee JH, Kossenkov AV, Wu SY, Wickramasinghe JM, Yin X, Palozola KC, Gardini A, Showe LC et al (2016) BET inhibitors suppress ALDH activity by targeting ALDH1A1 super-enhancer in ovarian cancer. Cancer Res 76(21):6320–6330
35. Ramadoss S, Sen S, Ramachandran I, Roy S, Chaudhuri G, Farias-Eisner R (2017) Lysine-specific demethylase KDM3A regulates ovarian cancer stemness and chemoresistance. Oncogene 36(11):1537–1545
36. Laury AR, Hornick JL, Perets R, Krane JF, Corson J, Drapkin R, Hirsch MS (2010) PAX8 reliably distinguishes ovarian serous tumors from malignant mesothelioma. Am J Surg Pathol 34(5):627–635
37. Jia L, Wang Y, Wang CY (2021) circFAT1 Promotes cancer stemness and immune evasion by promoting STAT3 activation. Adv Sci (Weinh) 8(13):2003376
38. Chen MW, Yang ST, Chien MH, Hua KT, Wu CJ, Hsiao SM, Lin H, Hsiao M, Su JL, Wei LH (2017) The STAT3-miRNA-92-Wnt signaling pathway regulates spheroid formation and malignant progression in ovarian cancer. Cancer Res 77(8):1955–1967
39. Bareiss PM, Paczulla A, Wang H, Schairer R, Wiehr S, Kohlhofer U, Rothfuss OC, Fischer A, Perner S, Staebler A et al (2013) SOX2 expression associates with stem cell state in human ovarian carcinoma. Cancer Res 73(17):5544–5555
40. Condello S, Morgan CA, Nagdas S, Cao L, Turek J, Hurley TD, Matei D (2015) β-Catenin-regulated ALDH1A1 is a target in ovarian cancer spheroids. Oncogene 34(18):2297–2308
41. Liu M, Wang Q, Shen J, Yang BB, Ding X (2019) Circbank: a comprehensive database for circRNA with standard nomenclature. RNA Biol 16(7):899–905
42. Wu W, Ji P, Zhao F (2020) CircAtlas: an integrated resource of one million highly accurate circular RNAs from 1070 vertebrate transcriptomes. Genome Biol 21(1):101
43. Dudekula DB, Panda AC, Grammatikakis I, De S, Abdelmohsen K, Gorospe M (2016) CircInteractome: a web tool for exploring circular RNAs and their interacting proteins and microRNAs. RNA Biol 13(1):34–42
44. Hu C, Xia R, Zhang X, Li T, Ye Y, Li G, He R, Li Z, Lin Q, Zheng S et al (2022) circFARP1 enables cancer-associated fibroblasts to promote gemcitabine resistance in pancreatic cancer via the LIF/STAT3 axis. Mol Cancer 21(1):24
45. Zhang JF, He ML, Fu WM, Wang H, Chen LZ, Zhu X, Chen Y, Xie D, Lai P, Chen G et al (2011) Primate-specific microRNA-637 inhibits tumorigenesis in hepatocellular carcinoma by disrupting signal transducer and activator of transcription 3 signaling. Hepatology 54(6):2137–2148
46. Penuelas S, Anido J, Prieto-Sanchez RM, Folch G, Barba I, Cuartas I, Garcia-Dorado D, Poca MA, Sahuquillo J, Baselga J et al (2009) TGF-beta increases glioma-initiating cell self-renewal through the induction of LIF in human glioblastoma. Cancer Cell 15(4):315–327
47. Zheng X, Huang M, Xing L, Yang R, Wang X, Jiang R, Zhang L, Chen J (2020) The circRNA circSEPT9 mediated by E2F1 and EIF4A3 facilitates the carcinogenesis and development of triple-negative breast cancer. Mol Cancer 19(1):73
48. Tang Z, Kang B, Li C, Chen T, Zhang Z (2019) GEPIA2: an enhanced web server for large-scale expression profiling and interactive analysis. Nucleic Acids Res 47(W1):W556–W560
49. Lyu X, Zeng L, Shi J, Ming Z, Li W, Liu B, Chen Y, Yuan B, Sun R, Yuan J et al (2022) Essential role for STAT3/FOXM1/ATG7 signaling-dependent autophagy in resistance to Icotinib. J Exp Clin Cancer Res 41(1):200
50. Guo R, Jiang M, Wang G, Li B, Jia X, Ai Y, Chen S, Tang P, Liu A, Yuan Q et al (2022) IL6 supports long-term expansion of hepatocytes in vitro. Nat Commun 13(1):7345
51. Chiba T, Yamada M, Hashimoto Y, Sato M, Sasabe J, Kita Y, Terashita K, Aiso S, Nishimoto I, Matsuoka M (2005) Development of a femtomolar-acting humanin derivative named colivelin by attaching activity-dependent neurotrophic factor to its N terminus: characterization of colivelin-mediated neuroprotection against Alzheimer's disease-relevant insults in vitro and in vivo. J Neurosci 25(44):10252–10261
52. Zhou S, Dai Q, Huang X, Jin A, Yang Y, Gong X, Xu H, Gao X, Jiang L (2021) STAT3 is critical for skeletal development and bone homeostasis by regulating osteogenesis. Nat Commun 12(1):6891
53. Chen L, Kong R, Wu C, Wang S, Liu Z, Liu S, Li S, Chen T, Mao C, Liu S (2020) Circ-MALAT1 functions as both an mRNA translation brake and a microRNA sponge to promote self-renewal of hepatocellular cancer stem cells. Adv Sci (Weinh) 7(4):1900949
54. Gao W, Guo H, Niu M, Zheng X, Zhang Y, Xue X, Bo Y, Guan X, Li Z, Guo Y et al (2020) circPARD3 drives malignant progression and chemoresistance of laryngeal squamous cell carcinoma by inhibiting autophagy through the PRKCI-Akt-mTOR pathway. Mol Cancer 19(1):166
55. Feng ZH, Zheng L, Yao T, Tao SY, Wei XA, Zheng ZY, Zheng BJ, Zhang XY, Huang B, Liu JH et al (2021) EIF4A3-induced circular RNA PRKAR1B promotes osteosarcoma progression by miR-361-3p-mediated induction of FZD4 expression. Cell Death Dis 12(11):1025
56. Friedman RC, Farh KK, Burge CB, Bartel DP (2009) Most mammalian mRNAs are conserved targets of microRNAs. Genome Res 19(1):92–105
57. Que T, Song Y, Liu Z, Zheng S, Long H, Li Z, Liu Y, Wang G, Liu Y, Zhou J et al (2015) Decreased miRNA-637 is an unfavorable prognosis marker and promotes glioma cell growth, migration and invasion via direct targeting Akt1. Oncogene 34(38):4952–4963
58. Wang L, Jiang F, Xia X, Zhang B (2019) LncRNA FAL1 promotes carcinogenesis by regulation of miR-637/NUPR1 pathway in colorectal cancer. Int J Biochem Cell Biol 106:46–56
59. Spitzner M, Roesler B, Bielfeld C, Emons G, Gaedcke J, Wolff HA, Rave-Frank M, Kramer F, Beissbarth T, Kitz J et al (2014) STAT3 inhibition sensitizes colorectal cancer to chemoradiotherapy in vitro and in vivo. Int J Cancer 134(4):997–1007